UNIVERSITY OF CALIFORNIA,

IRVINE

Nanopores and Micropores as Tools for Biomimetics and Biotechnology

DISSERTATION

Submitted in partial satisfaction of the requirements

for the degree of

DOCTOR OF PHILOSOPHY

in Physics

by

Laura Michele Innes

Dissertation Committee:

Professor Zuzanna Siwy, Chair

Professor Michael Dennin

Professor Ken Shea

2015

DEDICATION

For my family past, present and future.

TABLE OF CONTENTS

LIST OF FIGURES

ACKNOWLEDGEMENTS

I would like to express a humungous amount of gratitude to my committee chair Zuzanna Siwy. Without your support and guidance I could not have achieved this.

I would also like to NSF Lifechips program and the Chao Family Cancer Center for the funding.

CURRICULUM VITAE

Laura Innes

EDUCATION

University of California, Irvine
Ph.D., Chemical and Materials Physics **Summer 2015**
Nanopores and Micropores as Tools for Biomimetics and Biotechnology
Advisor: Professor Zuzanna Siwy

University of California, Irvine
M.S., Chemical and Materials Physics **2014**
Hydrophobic Gating in Single and Multiple Nanopores
Advisor: Professor Zuzanna Siwy

University of California, Irvine
Bachelors of Science/Arts, Physics and International Studies, **06/2010**

EXPERIENCE

SIWY LAB, University of California, Irvine **06/2011-Present**
Graduate Student Researcher – Department of Physics and Astronomy
Led multiple research projects with nanopores and developed cutting edge medical devices.

- Developed a novel technology that improves the detection and characterization of circulating tumor cells by mechanical properties and chemical affinity, which resulted in the filing of a patent.
- Developed and tested prototypes for the cell detection device and performed statistical analysis of millions of data points to elucidate trends.
- Research with bead system mimics of the cell solutions lead to a high impact journal publication and two presentations at Biophysical Society Meeting 2015 and Pittcon 2015.
- Studied ion transport properties of carbon nanotube devices and presented at collaboration meetings.
- Improved fabrication process tenfold for creating hydrophobic gates being studied for possible drug delivery applications. This project resulted in the writing of a Master's Thesis and a high impact journal publication.
- Led a team of graduate students in fabrication, collection and analysis of data for the hydrophobic gate resulting in a high impact journal publication.
- Created a system to mimic the hydrophobic nature of glycol-proteins to better understand their transport behavior in the body allowing researchers to design more effective cancer drugs. Presented research at collaboration meetings.

UNIVERSITY OF CALIFORNIA, IRVINE, Irvine, CA **09/2010-06/2011**
Teaching Assistant
Mentored and trained undergraduate students in introductory physics through weekly presentations

- Received high marks from evaluations for ability to communicate and explain topics

SIWY LAB, University of California, Irvine **09/2006 - 06/2010**
Undergraduate Research Assistant

Conducted independent research projects while maintaining full class schedule

- Studied oscillations between open and closed states in nanopores due to nanoprecipitaiton and the similarity in the open and close states in biological channels resulting in high impact journal publication.

PUBLICATIONS

Laura M Innes, Diego Gutierrez, William Mann, Steven F. Buchsbaum, and Zuzanna S. Siwy, Presence of Electrolyte Promotes Wetting and Hydrophobic Gating in Nanopores with Residual Surface Charges Analyst (2015)

Chin-Chang Kuo, Yongxue Li, Du Nguyen, Steven Buchsbaum, **Laura M Innes**, Aaron P. Esser-Kahn, Lorenzo Valdevit, Lizhi Sun, Zuzanna Siwy, and Michael Dennin Macroscopic strain controlled ion current in an elastomeric microchannel**,** Journal of Applied Physics, 117, 174904 (2015)

Laura M Innes , Chin-Hsuan Chen , Matthew Schiel , Matthew Pevarnik , Florian Haurais , Maria Eugenia Toimil-Molares , Ivan V Vlassiouk , Luke S. Theogarajan , and Zuzanna S. Siwy, Velocity Profiles in Pores with Undulating Opening Diameter and Their Importance for Resistive-Pulse Experiments Analytical Chemistry, 86 (20), 10445–10453 (2014)

Laura M Innes, M.R. Powell, I. Vlassiouk, C. Martens, Z.S. Siwy, Precipitation Induced Voltage-Dependent Ion Current Fluctuations in Conical Nanopores Journal of Physical Chemistry C, 114, 8126-8134 (2010)

PRESENTATIONS

Laura M. Innes, Ashley Fong, Matthew Pevarnik, Matthew Schiel, Eugenia Toimil-Molares, Luke Theogarajan, Christopher Hughes, Zuzanna Siwy Deformation of MCF-7 Cells in Micropores with Undulating Diameter 59th Annual BPS Meeting, Baltimore, MD, United States, February 7 – February 11, 2015

Laura M. Innes, Ashley Fong, Matthew Pevarnik, Matthew Schiel, Eugenia Toimil-Molares, Luke Theogarajan, Christopher Hughes, Zuzanna Siwy Pores with Undulating Diameter for Multipronged Characterization of Single Particles in Resistive-Pulse Technique Pittcon 2015, New Orleans, LA, United States, March 8 – March 12, 2015

Laura M. Innes, Ashley Fong, Matthew Pevarnik, Matthew Schiel, Eugenia Toimil-Molares, Luke Theogarajan, Christopher Hughes, Zuzanna Siwy Deformation of Biological Cells in Micropores with Undulating Diameter 16th Annual UC System Wide Bioengineering Symposium , Santa Cruz, CA, United States, June 22 – June 24, 2015

HONORS, AWARDS, and Affiliations

- Association of Graduate Students 2014 Symposium best interdisciplinary research presentation
- Lifechips Fellow
- NSF Honorable Mention 2012

- IMSURE Fellow
- UROP Fellow
- Biophysical Society Member
- Sigma Pi Sigma
- National Society of Collegiate Scholars

ACTIVITIES AND LEADERSHIP

PAUL MERAGE SCHOOL OF BUSINESS, BUSINESS PLAN COMPETITION **05/2013**

- Led cross-functional team that won third place overall and the Life Sciences Award for the development of a novel medical device for the detection of circulating tumor cell. Interacted with cancer researchers and doctors for market analysis. ($33,500)(~200 applicants)

WOMEN IN PHYSICS AT UCI GROUP **06/2013 – 06/2015**

- Founded group to promote community and increase retention of women in physics
- Increased membership up to 70 based on marketing efforts and programming

ABSTRACT OF THE DISSERTATION

Nanopores and Micropores as Tools for Biomimetics and Biotechnology

By

Laura Michele Innes

Doctor of Philosophy in Physics

University of California, Irvine, 2015

Professor Zuzanna Siwy, Chair

Nanopores and micropores are of great interest as tools in biomimetics and biotechnology. Pores used in this study were prepared by the track-etching technique in polymer foils of polyethylene terephthalate and polycarbonate. Opening diameter of these pores can be tuned from a few nanometers up to tens of micrometers. Nanopores in polyethylene terephthalate were used as a model system for understanding hydrophobic interactions at the nanoscale. Walls of these pores were decorated with alkyl chains of varying length between three and ten carbon atoms. We show that hydrophobic interactions are not only tuned by the pore opening diameter, but also type of chemical modification and electrolyte ionic strength. More concentrated solutions favored wetting of the pores so that finite ion current could be recorded. We also used micrometer sized pores in polyethylene terephthalate and polycarbonate pores as a tool for detecting microspheres and biological cells. We focused on the influence of local diameter undulations of the pores on the object transport. We found that rough forms feature local pressure gradients, which can be used to

probe mechanical properties of translocating objects. Potential application of such pores for detecting circulating tumor cells is discussed.

Chapter 1
Introduction

Nanopores and micropores are of great utility to the scientific community. They can be used as tools to study ionic and molecular transport at the nano and microscale, as sensors for biomolecules and even as mimics of biological channels in a cell membrane [1], [2]. Though similar in design, nano and micropores lend themselves to completely different applications by virtue of their size. Micropores have been used extensively to detect and characterize biological structures such as cells while nanopores have been used to study ions and molecules.

Biological channels offer superior control over the flow of ions and water, something that scientists have been attempting to duplicate with man-made systems. Many biological channels use hydrophobic residues to control these flows [3], [4]. Thus an understanding of hydrophobic interactions on the nanoscale is important and nanopores offer a tool to study these interactions. The control of water, ions and molecules at nanoscale is important for the creation of on demand drug delivery systems, nonlinear circuits and biosensors [5], [6].

Micropores have been used for many years as a template for the detection of biological cells, as with the Coulter counter technique used to analyze blood samples [7]. Progress in microfabrication has allowed for the creation of pores with different geometrical properties, which induce interesting and non-trivial fluid flows [8]. These nontrivial flows expand the capabilities of the micropore system for fluid control. Objects in the flow can now be characterized based on physical properties such as size, shape, and even mechanical properties.

This line of research is especially interesting for probing biological cells. Abnormal physical properties of cells can be indicative of disease, such as the shape of the red blood cells in

sickle cell anemia or the increased rigidity of red blood cells in malaria [9], [10]. There is also a growing interest in correlating physical properties of cancer cells with their malignancy. Cancer cells have already been shown to be larger than other cells in the blood [11] and squishier than healthy cells; increased squishiness was correlated with increased metastatic potential of the cells [12]. Cancer cells can also have a different response to external electric field. For example, the more metastatic prostate and breast cancer cells were found to have higher motility in an applied electric field [13]. Finally cancer cells have a different shape than benign cells [14]. These features may allow for the design of a microfluidic device capable of characterizing the physical properties of individual cells with applications in cancer diagnosis and therapy.

1.1 Hydrophobicity in Biological Channels and Synthetic Mimics

Mechanisms for the regulation of transport in biological and synthetic nanopores can be grouped into three different categories, based on steric, electrostatic, and hydrophobic interactions [15]. Steric interactions allow channels to exclude molecules or ions based on their size. Thus only ions or molecules small enough too sterically fit into the constriction can pass through, similar to a mechanism of a molecular sieve. Electrostatic interactions exclude ions and molecules based on their charge. A channel with positive surface charges will primarily transport negative species, rejecting the positive ones. Similarly, a negative channel will transport mostly positive ions or molecules. Hydrophobic interactions, which will be the focus of this thesis, hinder the transport of water and any species dissolved in it.

Hydrophobic interactions are used in some biological channels to control water and ion transport [16]. This mechanism in mechanosensitive channels has been known for some time, while it is a recent discovery in voltage-gated potassium channels [4]. Though, mechanosensitive channels open and close with mechanical stress in the membrane and voltage-gated potassium

channels open and close with trans-membrane voltage, they both use hydrophobic residues to help control the flow of water. In a mechanosensitive channel, specifically the MscL tension channel in E. coli, Figure 1.1, the channel is in a closed state when there is no stress in the membrane [17]. This closed state occurs due to clustering of the hydrophobic helices, shown as yellow rods in Figure 1.1. When the hydrophobic helices are close together they prohibit water from being able to move through the channel. However when there is stress in the membrane, forcing the helices apart, the water fills the channel allowing the transport of water and ions.

The voltage gated potassium channel is comprised of a voltage sensing domain, S4 helix,

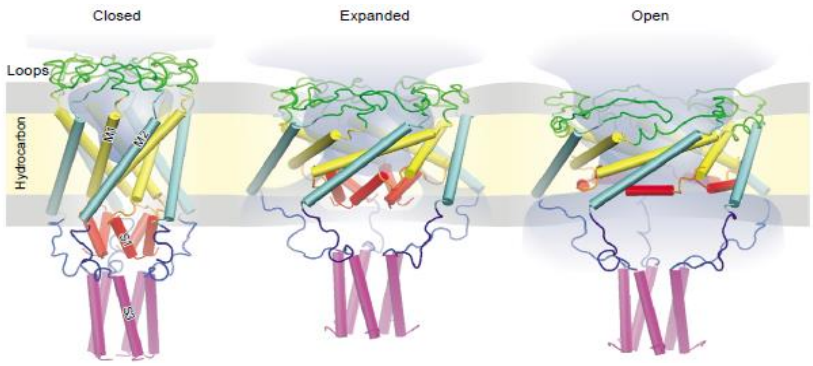

Figure 1.1: Visual representation of the MscL tension channel in E. coli. The hydrophobic helices are represented by yellow rods. When they are close together a tight gate is formed preventing water and ions from being transported [17].

a pore and a cavity, Figure 1.2 [16]. As the pore is closing the hydrophobic residues in the channel move closer together causing water to leave the channel. Upon the application of voltage the S4 helix is moved up pulling the pore open. This forces the hydrophobic residues apart allowing for the transport of water and potassium ions.

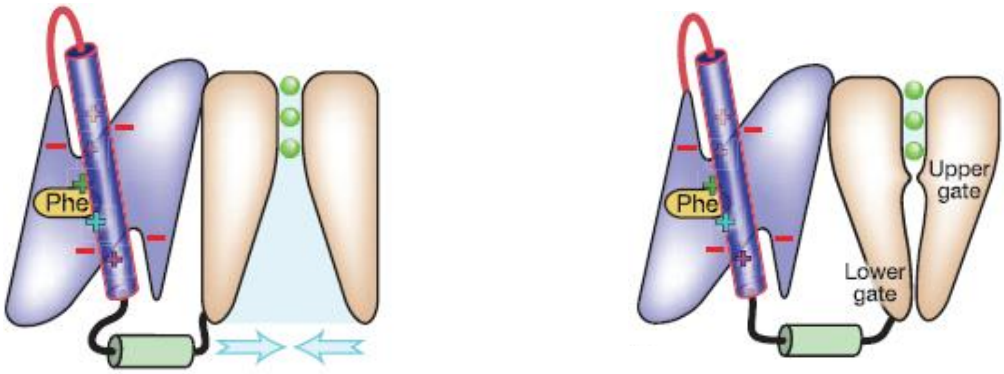

Figure 1.2: Voltage-gated potassium channel. **A)** Voltage sensing rod is pulled up allowing the flow of potassium ions and water. **B)** Voltage sensing rod is down and the pore is in a closed state preventing the flow of water and potassium ions [16].

A better understanding of how biological channels use hydrophobic interactions to regulate the flow of water aids in the creation of a synthetic mimic of a hydrophobically gating nanopore. Hydrophobic interactions in nanopores allow for the control of the transport of water and all species dissolved in it even without moving parts. The density of water close to hydrophobic surfaces has been found to be lower than in bulk [18]. It was further predicted that a sufficiently narrow hydrophobic nanopore will facilitate spontaneous evaporation of water, creating basis for hydrophobic gating [19]. Thus the small opening size and ability to make the nanopores hydrophobic result in a closed state prohibiting the transport of water and ions through the pore. Transport could be resumed if an external stimulus in a form of pressure or electric potential gradient was applied across the pore. Removing the stimulus would be followed by water evaporation and the transport would cease until arrival of another stimulus.

Creating an open state of a hydrophobic nanopore indeed requires the application of external stimuli. Most experiments with hydrophobic nanopores use outside pressure to force the condensation of the water vapor inside the pore [20], [21]. The first experimental demonstration of hydrophobic gating in nanopores using an externally applied electric field was reported by

Powell et al [22] and Smirnov et al [23]. Figure 1.3A shows current-voltage curves through a 16 nm nanopore whose walls were modified with modestly hydrophobic methyl esters. The pore remained closed for ionic transport until a threshold voltage was reached. The state with zero current was believed to correspond to the pore totally or partially filled with water vapor. When finite values of currents were observed the whole pore length was filled with condensed water. Lowering the voltage closed the pore for ionic transport again. Figures 1.3B and C indicate that the pore underwent repeatable switching between open and closed states however the voltages at which the transitions occurred varied between scans. Thus further research was found necessary as to optimize the pore surface modification to assure more reproducibility.

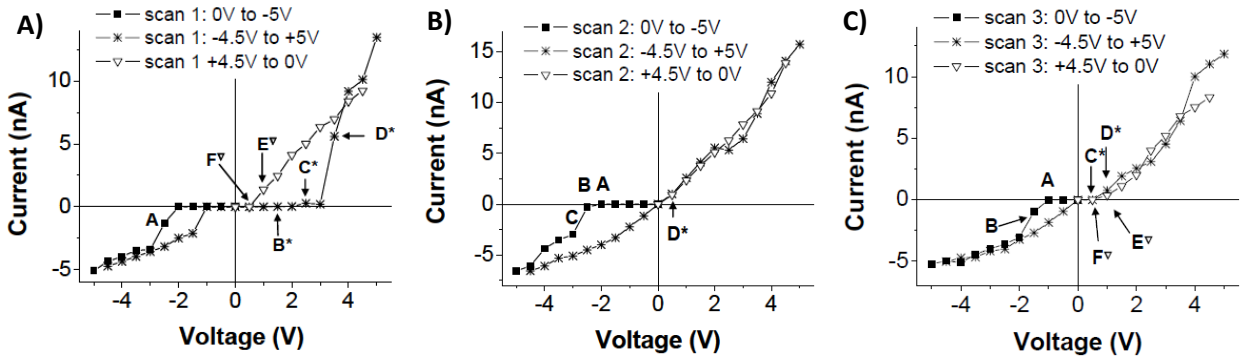

Figure 1.3: Current-voltage curves for a single 16 nm in diameter conically shaped polyethylene terephthalate (PET) nanopore modified with 5 mM trimethylsilyldiazomethane for 15 minutes. **A)** First forward and reverse scans indicated existence of hydrophobic gating thus voltage induced switching between conductive and non-conductive states. Subsequent scans are shown in **B)** and **C)** [22].

1.2 Physical Characteristics of Biological Cells: A Closer Look at CTC Detection

Abnormal physical characteristics of cells are often indicative of disease, such as red blood cells in sickle cell anemia and malaria. Presence of tumor cells in blood, so called circulating tumor cells (CTCs) is indicative of metastatic cancer. In sickle cell anemia and malaria a simple blood test can be performed to diagnose the disease, because red blood cells are abundant thus easy to capture and characterize [9], [10]. Detection of CTCs however is much more challenging due to

the cells' rarity. There can be as few as 10 CTCs per mL of blood comingled with billions of red blood cells and millions of white blood cells, making their detection very difficult. CTCs are cells which are shed from a solid tumor and manage to enter the blood stream [24]. Once in the blood they can travel to any other organ in the body and seed a secondary tumor, Figure 1.4. Counting the number of CTCs in a patient's blood before and after a course of treatment can aide in the prognosis of the patient and help choose the most effective treatment. More importantly, isolating these cells would become a basis of minimally invasive 'liquid' biopsy of the tumor and could provide further insight into which medications and treatments are best suited for that specific patient *before* administering it to the patient. To reach the full potential of the technique, the isolated cells need to be isolated in a non-destructive manner so that viable CTCs could be subjected for further testing and lead to true personalized medicine.

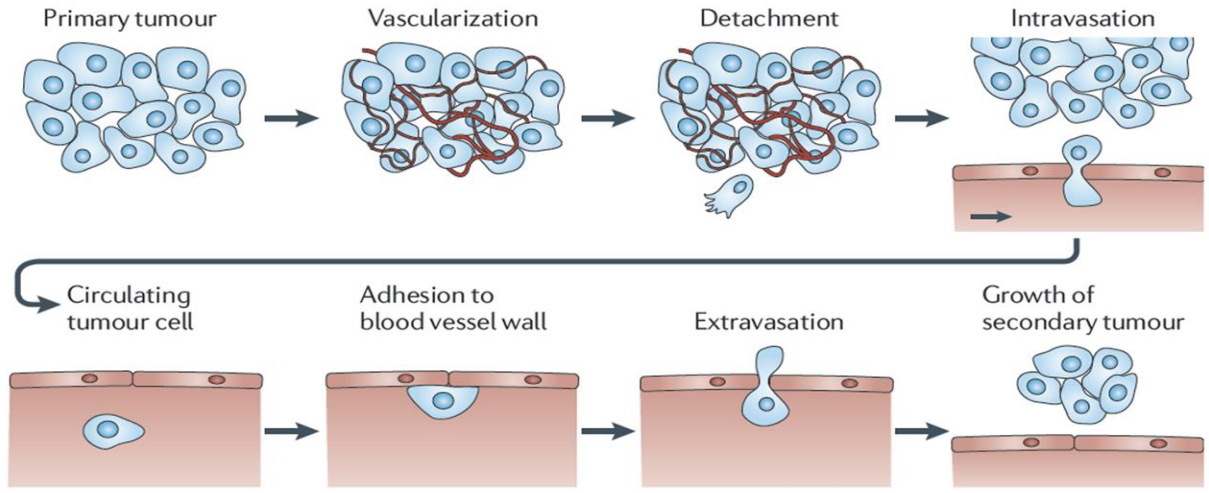

Figure 1.4: Visualization of cancer metastasis. After vascularization a cell is shed from the primary tumor and squeezes through the blood vessel walls (intravasation). Once in the blood stream the cell can travel through it, attach to the blood vessel walls and squeeze back through (extravasation), allowing it to seed a secondary tumor [24].

Veridex's Cell Search is the only FDA approved device for counting CTCs is based on a biomarker Epithelial Cell Adhesion Molecule (EpCAM) which many types of cancers overexpress [25]. The isolated cells are however not viable limiting the utility of the approach for the

development of patient specific treatment. Most importantly, cancers in late stages often do not overexpress EpCAM and some cancers e.g. melanoma do not express the marker at all. There has been therefore a growing interest in the community to develop non-destructive methods that would be agnostic thus applicable to various types of cancer. An approach based on physical properties of CTCs has been found especially promising. One direction uses the size disparity between CTCs and other blood components. Fabrication of microfilters with well-defined pore size and their application for CTCs capture have been reported, [26], [27], Figure 1.5B. This device however would not be able to detect cancer cells smaller or comparable in size than white blood cells, and the captured population might be contaminated with large white cells. In addition, larger more deformable CTCs would not be isolated either. Another set of devices utilizes the larger deformability/squishiness of CTCs, as shown for example by using optical forces in a microfluidic optical stretcher, Figure 1.5C [28] and atomic force microscopy [29]. Figure 1.5D [30] shows a microfluidic channel with constriction significantly smaller than the cells' diameter. The time each cell needed to enter the channel under applied pressure difference was correlated with metastatic potential. This approach however subjected the cells to high shear stresses and was destructive to the cells.

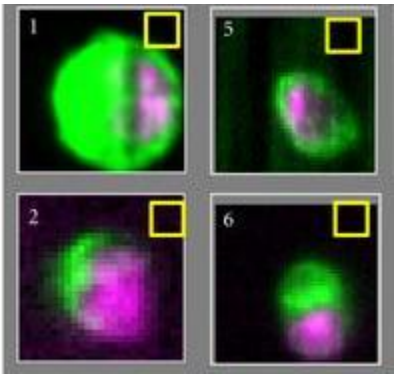

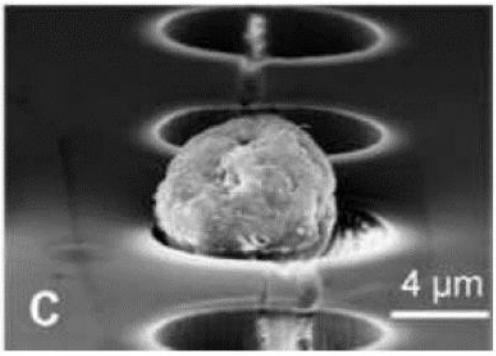

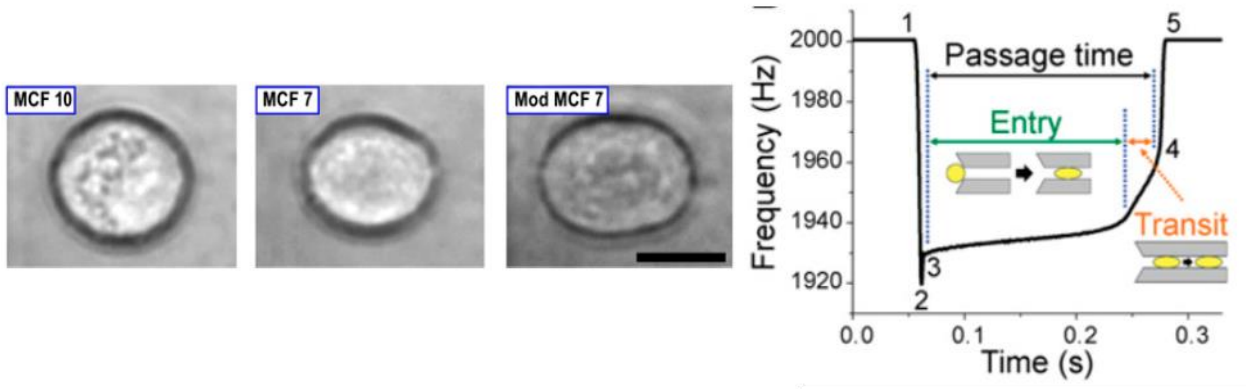

Figure 1.5: CTC separation techniques **(A)** Separation of CTCs with EpCAM using Veridex's Cell Search. Image of possible CTCs dyed with DAPI purple and CK-PE green [25]. **(B)** CTC separated using microfilter [26] **(C)** Images of MCF 10, MFC 7 and Mod MCF 7 cells being deformed with optical forces [28]. **D)** Graph of passage time for CTC through microchannel with inset of visual representation of cell passage [30].

It would therefore be advantageous to develop a multipronged approach to CTCs characterization and detection such that each cell would be characterized by a set of physical properties. This would allow one to identify a physical fingerprint for various types of cancers and provide a method for non-destructive characterization and isolation of the cells. It will be shown in this thesis how passing cells through rough microchannels can offer the possibility to characterize individual objects by size, mechanical properties and surface charge.

Chapter 2
Nanopore and Micropore Fabrication

The nano and micropores used in these experiments were created using the track-etch technique in both polyethylene terephthalate (PET) and polycarbonate (PC) foils. This process

starts at the GSI Helmholtzzentrum für Schwerionenforschung linear accelerator in Darmstadt, Germany, where the latent damage track is created. The pore is then fabricated in the lab by chemically etching the irradiated foils. For preparation of nanopores with hydrophobic gating mechanism, single conically shaped nanopores in 12 μm thick PET foils were fabricated. The resistive pulse experiments were performed with cylindrically shaped micropores in both PET and PC foils with thicknesses between 12 μm and 100 μm.

2.1 Latent Damage Track Creation, Pore Formation and Characterization

The first step of the track-etch technique is the creation of the latent damage track in the foil. The latent damage track is created in both the PET and PC foils through irradiation by swift heavy gold or uranium ions in the linear accelerator UNILAC at GSI Helmholtzzentrum für Schwerionenforschung in Darmsadt, Germany. The ions used for this irradiation have a total kinetic energy of 2 GeV and the deposition of this energy creates the damage track[31]. The number of damage tracks can be controlled from 1 to 10^{10} per cm^2. A single damage track results in a single pore after chemical etching [32]. After the correct number of ions pass through the foil, the beam is switched off and the next set of foils is moved to the beam. In all discussed in the thesis experiments, foils with a single damage track were used. The second step in this process is to expose the foil to longwave ultraviolet (UV) light for one hour on each side. Irradiation by UV light "ages" the damage track in the foil, resulting in an etch time 3 times faster than untreated foils [33]. It has been suggested this sensitization might occur because of PET's strong absorption of wavelengths less than 310 nm [34].

In order to create a specific pore shape the two etching velocities need to be controlled. The bulk etch rate (v_b) dictates how fast the bulk material is etched, while the track etch rate (v_t)

controls how fast the etchant etches along the damage track, Figure 2.1. Elevated temperature of etching increases the track etch rate facilitating preparation of cylindrically shaped pores especially if a diluted solution of an etchant is used, Figure 2.1A.

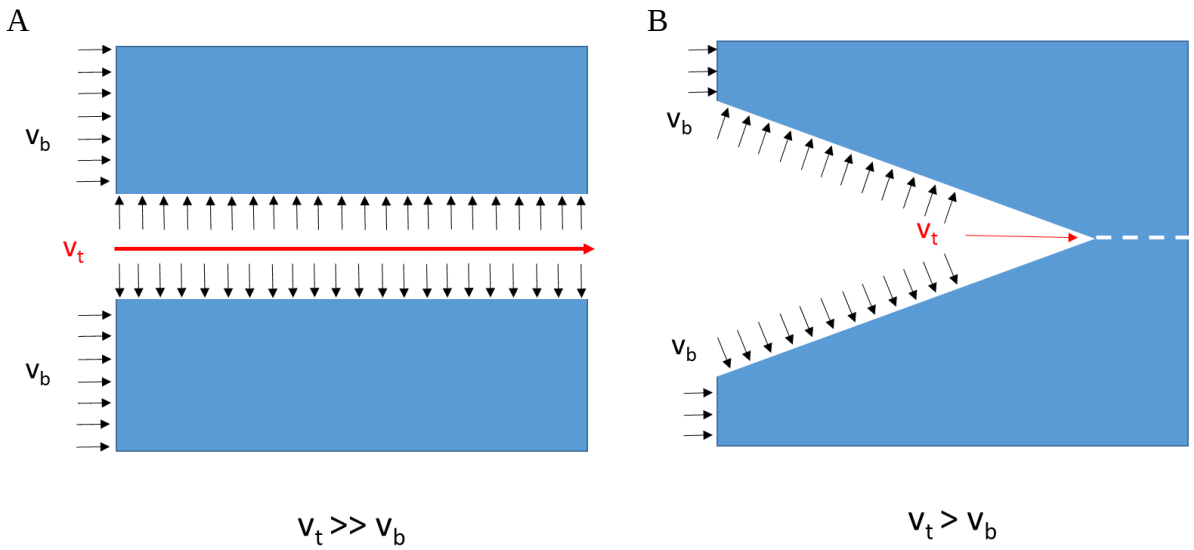

Figure 2.1: Comparison of bulk and track etch rates, v_b and v_t respectively, for two different pore geometries. **A)** Cylindrically shaped pores are etched at an elevated temperature in order to drastically increase the track etch rate compared to the bulk etch rate. **B)** Conically shaped pores are etched at room temperature in so that the track etch rate only a little larger than the bulk etch rate.

A different etching procedure was developed to prepare conically shaped nanopores. First the etching system needs to be asymmetric thus fabrication of conical nanopores is performed in a conductivity cell, Figure 2.2. Etching at room temperature slows down the track-etch rate, Figure 2.1B [35], [36]. The bulk etch rate is increased by using a concentrated etchant, which is 9 M NaOH for pores in PET. NaOH is placed on one side of the membrane in contact with the working electrode, and a stopping solution of 1 M formic acid and 1 M KCl is placed on the other side with the ground electrode. The etching process is monitored by applying 1 V across the membrane and measuring the current. The etching continues until a current of ~200 pA is achieved, which assures preparation of nanopores with an opening below 10 nm. Etching is then stopped by removing the 9 M NaOH, and rinsing the reservoirs with the stopping solution and water. Using NaOH to etch

PET and PC creates carboxyl groups on the walls of the pore giving them a negative surface charge for solutions above pH 4 [1].

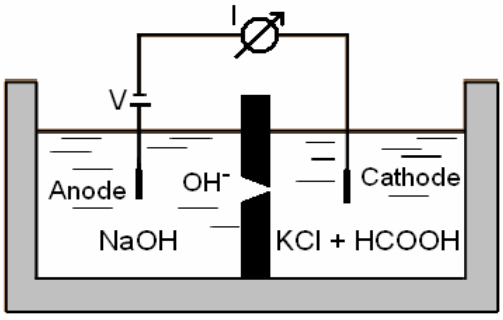

Figure 2.2: Setup for etching a conical nanopore in a conductivity cell.

Once the etching is completed, the pore is characterized electrochemically in a conductivity cell. The pore opening diameter is estimated by recording current-voltage (I-V) curve in 1 M KCl pH 8. The following formula relates the pore resistance, R, with its opening diameter (d) for a conical pore:

$$d = \frac{4L}{\kappa \pi R D} \quad [2.1]$$

where L the length of the pore, κ conductivity of 1 M KCl which is 10 S/m, R is the resistance of the pore which is determined through linear regression of the I-V curve, and D is the size of the large opening diameter which for PET is determined by the following equation [35]:

$$D = 2 * t * 2.13\ nm/min \quad [2.2]$$

t is the time of the etching and 2.13 nm/min is the bulk etch rate of PET in 9 M NaOH at room temperature. An example of a sizing I-V curve is seen in Figure 2.3.

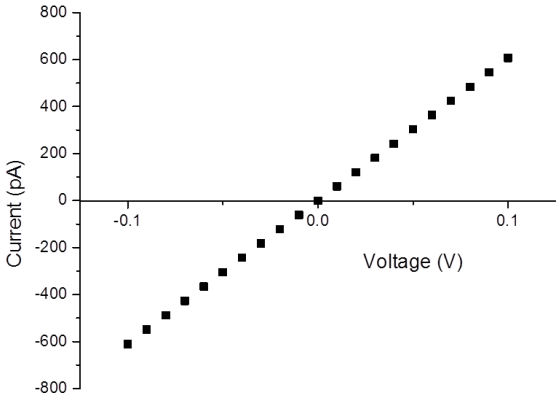

Figure 2.3: Current-voltage curve of a single conically shaped nanopore with a tip diameter of this pore was 9 nm.

To confirm the conical shape of nanopores, their metal replica can be created. This is done through electrodeposition or electroless deposition of a metal e.g. gold into the pores [37]. Figure 2.4A shows a gold replica of an electroless plated conical nanopore where the base diameter is indeed much larger than the tip diameter.

A nondestructive way to confirm the conical shape of a nanopore is to check for rectification of the ion current. Rectification of the ion current is a property such that currents for one voltage polarity are higher than ion currents for the opposite voltage polarity, Figure 2.4B. This ion current behavior is seen in conically shaped nanopores with surface charge because of the voltage modulations of ionic concentrations inside the pore due to the asymmetric shape and the charges on the walls. By lowering the pH of the solution to less than 4, the charges on the pore walls are neutralized and the rectification property of I-V curves is lost. This phenomenon will be discussed in more detail in Chapter 3.

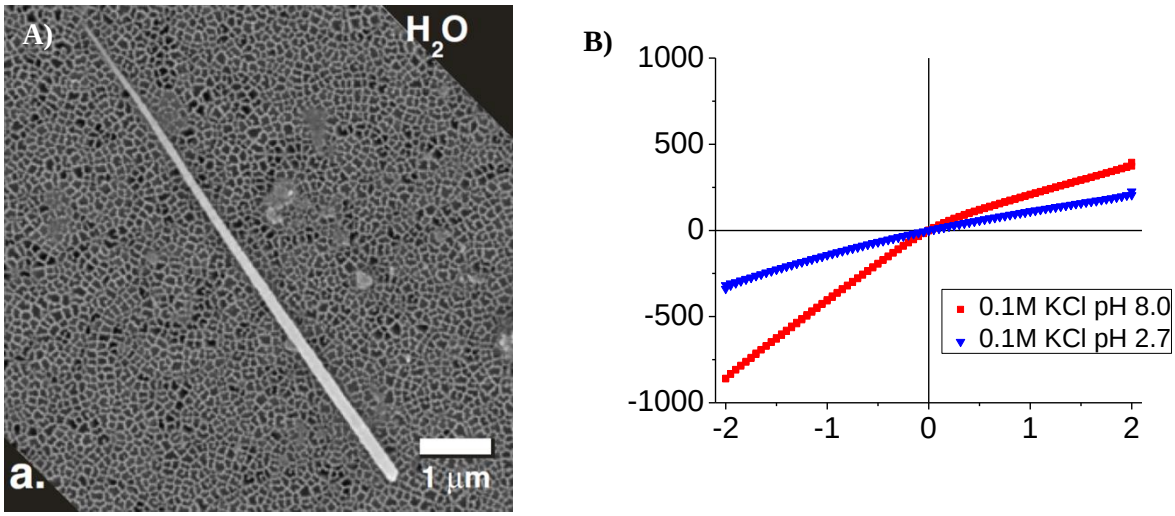

Figure 2.4: **A)** SEM image of a gold replica of a single conical nanopore, created by electroless deposition of gold [37]. **B)** IV curve for a 6 nm pore etched for 223 min recorded in 100 mM KCl pH 8 (red) and pH 2.7 (blue) [38].

Opening diameter of a cylindrically shaped pore can be found from:

$$D^2 = \frac{4L}{\kappa \pi R} \qquad [2.3]$$

where all the variables are the same as equation 2.1 except D now represents the average diameter of the pore. While track-etched PC pores have smooth pore walls and are indeed cylindrical in shape, pores in PET are very rough, translating into an axially varying diameter. This roughness stems from the semi-crystalline character of PET and its laminar structure, which leads to over etching of the material between the strata. In order to illustrate the 3D topography of the pores as a function of pore diameter, gold replicas were prepared by electrodeposition. Three multi-pore samples were etched for varying amounts of time resulting in pores that were 490 ± 40, 660 ± 30, and 1230 ± 70 nm in diameter. The gold wires in Figure 2.5 show the overall cylindrical shape of the pores and the irregularities of the channel diameter along the axis. Over 20 wires of each sample were examined. The analysis revealed that longer etching times promote the formation of smaller irregularities and a widening of the large cavities.

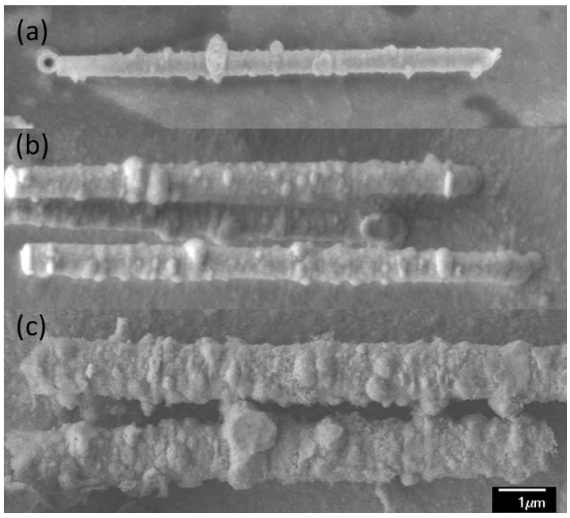

Figure 2.5: Metal replicas of PET pores to show that roughness increases with etch time. These pores were all etched in 0.5 M NaOH at 70 °C for the times listed below. The metal replicas were created by plating gold into multipore samples and etching the PET away. **A)** 490 nm pore that was etched for 146 minutes. **B)** 660 nm pore that was etched for 186 minutes. **C)** 1230 nm pore that was etched for 300 minutes [39].

2.2 Hydrophobic Modification of PET Nanopores

Three different amine modifications were performed to create hydrophobic regions in conically shaped PET nanopores using an Ethyl-3-(dimethylaminopropyl)carbodiimide (EDC) linker to attach aliphatic amines to carboxyls. EDC based conversion of carboxyls groups is not complete i.e. the walls of modified pores have regions of hydrophobic and hydrophilic groups. Modifications with propylamine, hexylamine, and decylamine were performed. These three alkyl chains were used to change the level of hydrophobicity of the modified regions. Propylamine is the least hydrophobic and decylamine is the most hydrophobic out of the three chemicals as dictated by the length of their carbon chains, Figure 2.6. PET foils without nanopores were modified in the same manner as the nanopores discussed below, and subjected to contact angle measurements, Figure 2.7.

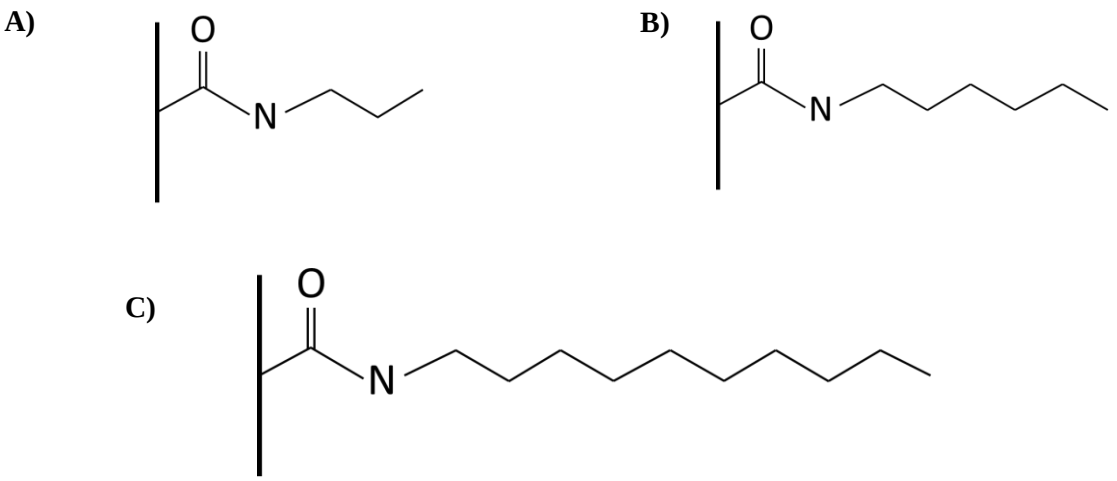

Figure 2.6: A) Propylamine **B)** Hexylamine **C)** Decylamine attached to a carboxyl group on the pore wall.

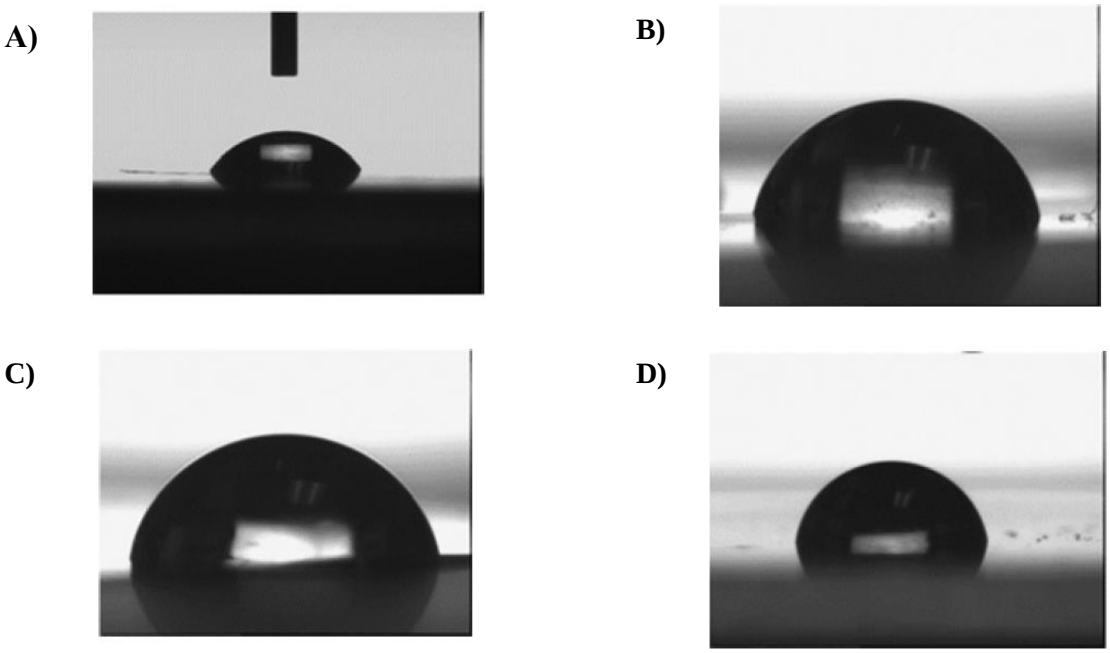

Figure 2.7: Contact angle measurements for **A)** Unmodified PET 58.0° ± 6.0° **B)** Propylamine 76.6° ± 5.8° **C)** Hexylamine 75.0° ± 3.4° **D)** Decylamine 79.4° ± 4.2°. All the modifications were done in the same way as the pores were modified. [39]

The chemical modifications of the nanopores were performed in a conductivity cell. A mixture of 0.2 M of pentafluorophenol (PFP) and 0.1 M of EDC in ethanol was prepared. This

EDC/PFP mixture was placed in reservoirs on both sides of the foil for one hour. During this hour EDC, an active intermediate, crosslinks the PFP, an amine reactive intermediate, with the carboxyl groups on the pore walls. After the reaction is complete, the reservoirs were rinsed with ethanol. Then a solution with 50 mM of either propylamine, hexylamine, or decylamine in ethanol is placed in the reservoirs. The reaction was run for 2 hours and then the solution was removed. The reservoirs were then rinsed with ethanol and followed by water.

Chapter 3

Transport Properties of Nanopores and Micropores

Understanding the transport properties of pores on the nano and microscales is important for the development of many of devices such as drug delivery systems and sensors for biomolecules and cells. Fundamental fluid physics on the micro and nanoscales can vary drastically from their macroscopic counterparts [8]. Thus nano and micropores offer a unique opportunity to study ionic transport and fluid dynamics on these small scales. The discussion below is divided into three parts: the study of ion transport through charged cylindrical nanopores, the examination of how changing the shape of a nanopore and chemical modification of the surfaces can modulate ion transport behavior, and the effect of electrokintetics on fluid velocities and particle transport in micropores.

3.1 Electrical Double Layer Formation and Ion Transport through Charged Nanopores

Ions can be transported via electric, concentration, pressure, and thermal gradients. Thermal and pressure gradients will not be considered here, as the system remained at room temperature and open to the atmosphere. In order to understand transport through a pore we will first analyze a charged planar surface and examine how the surface charges influence electric potential and ionic concentrations in the solution. When the system is in equilibrium, the electric potential distribution is given by the Poisson equation

$$\nabla^2\phi = \frac{-z\,C}{\varepsilon_r\varepsilon_0} \qquad [3.1]$$

where ε_r is the permittivity of water, ε_0 is the permittivity of free space, φ stands for the electric potential, z is charge of the ion species, and C is the concentration of net charges; e.g. for a negatively charged surface, C is the difference of concentrations of positive and negative ions. If we consider a 1-dimensional system, φ and C will be a function only of x where x is the distance from the charged wall.

Combining the Poisson equation with the Boltzmann distribution for ions, one gets the following equation for C(x):

$$C(x) = C_0 zF\left(e^{\frac{-ze\phi(x)}{k_B T}} - e^{\frac{ze\phi(x)}{k_B T}}\right) \quad [3.2]$$

$$= -2C_0\, z\, e \sinh\frac{ze\phi(x)}{k_B T} \quad [3.2a]$$

When the surface potential is smaller than $k_B T$, equation 3.2a can be linearized giving

$$C(x) = \frac{2z^2 e^2 C_0 \phi(x)}{k_B T} \quad [3.2b]$$

where k_B is the Boltzmann constant and T is the temperature. Applying the boundary conditions of $\phi(x) = 0$ as $x \to \infty$ and that $\phi(0)$ is equal to the potential at the surface, one gets the following equation for the potential:

$$\phi(x) = \phi_{surface} e^{\frac{-x}{\lambda}} \quad [3.3]$$

with

$$\lambda = \sqrt{\frac{k_B T \varepsilon_r \varepsilon_0}{2z^2 e^2 C_0}} \qquad [3.4]$$

where z is the charge of the ion, e the charge of an electron, and C_0 stands for the bulk concentration. The Debye length, λ, is therefore the distance from the pore walls over which the surface electric potential decays e times (Figure 3.1); it is thus often considered a distance over which electrostatic interactions are screened. At room temperature in 100 mM KCl solution in water λ = 1 nm. The Stern layer and the Debye layer together are often referred to as the electrical double layer (EDL). The Stern layer is the immobile layer of counter ions on the charged surface and the Debye layer is a layer of diffuse ions consisting mostly of counter ions which can contribute to ion current when external electric field is applied.

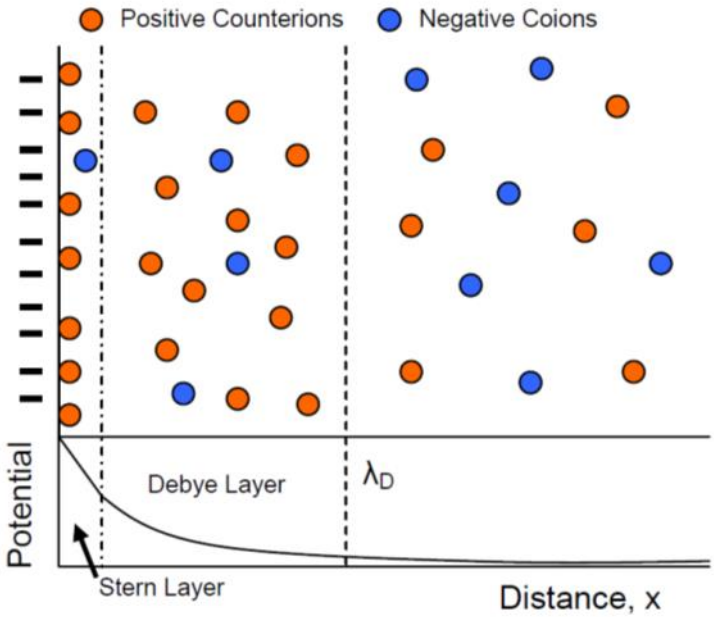

Figure 3.1: Visual representation of the electrical double layer of a charged flat surface, where the Stern layer is the immobile layer of counter ions on the charged surface and the Debye length represents the distance at which the counter ions dominate [40].

The Poisson-Boltzmann equation also predicts distribution of cations and anions in the solution. For a negatively charged surface the concentration of cations will be very high close to the surface and decrease exponentially to the bulk value with distance. The concentration of anions

will increase from a low value at the surface to the bulk level. In order to describe ion current, we will first consider ionic flux induced by gradients of concentration and electric potential given by the Nernst-Planck equation.

$$J_i = -D_i \left(\nabla C_i + \frac{z_i e C_i}{k_B T} \nabla \phi \right) \quad [3.5]$$

J_i is the flux of each ion species with the charge z_i (i = + or -), D_i is the diffusion coefficient, C_i is the concentration of each of the ion species. The steady state solution of interest satisfies the continuity equation

$$\nabla \cdot (C_i u + J_i) = 0 \quad [3.6]$$

where the velocity vector is represented by u. Assuming the fluid is incompressible indicates that

$$\nabla \cdot u = 0 \quad [3.7]$$

To complete the set of equations Navier-Stokes needs to be added

$$u \nabla u = \frac{1}{\rho} [-\nabla p + \nu \nabla^2 u - (C_+ - C_-) \nabla \phi] = 0 \quad [3.8]$$

The mass density is represented by ρ and υ is the viscosity of the solution. The complete set of the Poisson-Nernst-Planck (PNP), and Navier-Stokes (NS) equations is very difficult to solve numerically thus often only PNP is considered whenever it is possible to assume that the solution velocity is zero:

$$\nabla \cdot \left(\nabla C_i + \frac{z_i e C_i}{k_B T} \nabla \phi \right) = 0 \quad [3.9]$$

In order to solve the equations numerically for a nanopore, the boundary conditions are set such that ϕ, C_i and their first derivatives are continuous except for the derivative of the electric potential at the pore wall equal to:

$$\left.\frac{d\phi}{dr}\right|_{r=a} = \frac{\sigma}{\varepsilon\varepsilon_0} \qquad [3.10]$$

Figure 3.2 shows numerical solutions of ionic concentrations and electric field along the axis of a single nanopore with an opening diameter of 8 nm, length of 128 nm and surface charge density -0.5 e/nm^2. As predicted from the analysis of a planar charged surface, with negative surface

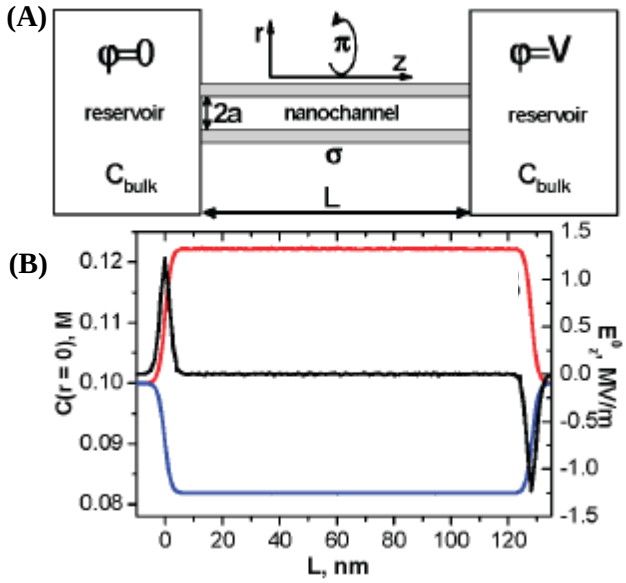

Figure 3.2: (A) Schematic of the nanochannel setup where C_{bulk} is the salt concentration, a is the radius, σ is the surface charge, and L is the length of the nanochannel. **(B)** Numerical solution of the PNP equations with the concentration of Cl^- represented by the blue line, concentration of K^+ in red, and the black line is the electric field at the center of the pore (r = 0). C_{bulk} = 0.1 M, L = 128 nm, a = 4 nm, σ = -0.5 e/nm^2 and the applied voltage is zero. The modeling was performed using Comsol [41].

charges on the pore walls, there is an enhanced concentration of cations, while anions are depleted. The degree of the modulations of ionic concentrations was however unexpected. The simulations were performed in 100 mM KCl thus in conditions in which the linearized theory predicts the Debye length of only 1 nm. Although the nanopore had an opening diameter of 8 nm, we still observed a significant difference in concentrations between cations and anions. These results

indicate that charged surfaces modulate concentration and electric potential over distances which are larger than the classically calculated Debye length.

3.2 Ion Transport in Conical Nanopores

Properties of ion transport can be further manipulated by changing the pore geometry. As mentioned above, the charges on the walls increase the concentration of counterions inside the pore above the bulk concentration. In long cylindrical nanopores this enhancement is electric field independent. When the pore is conical in shape the concentration of both cations and anions is not only dependent on the magnitude of voltage but also on its polarity so that ion current rectification is observed. Figure 3.3 shows results of numerical modeling performed for a conically shaped nanopore with opening diameters of 5 nm and 500 nm and a length of 12 μm. We show concentrations of potassium and chloride ions along the pore axis for a range of voltages between -1 V and +1 V. When the positively biased electrode is on the same side as the small opening of the pore the cations will move toward the large opening and the concentration of both types of ions is enhanced above the bulk concentration. This concentration enhancement causes a larger magnitude of current to be observed. For the opposite voltage polarity, there is a depletion zone created which limits the ionic flow and creates a system with a lower conductance.

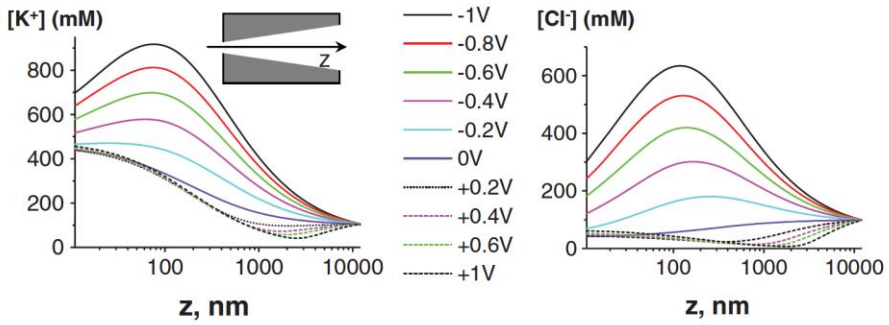

Figure 3.3: Concentration of potassium and chloride ions modeled by numerically solving PNP equations for a conically shaped nanopore with an opening diameter of 5 nm and 500 nm, bulk concentration is 0.1 M KCl [42].

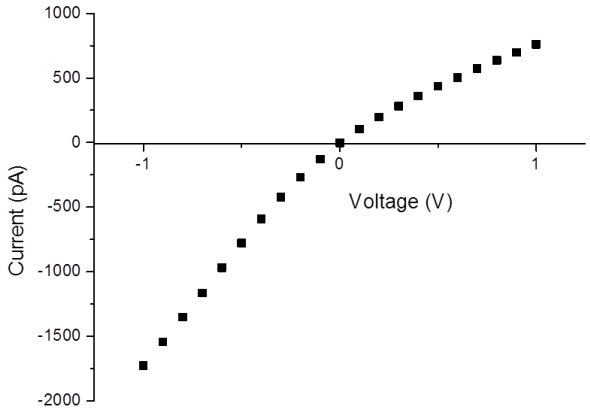

Figure 3.4: Current-voltage curve of a 9 nm conical nanopore in 100 mM KCl.

3.3 Transport Behaviors with Surface Modifications

3.3.1 Tuning surface charge of the pore walls

Chemically modifying walls of nanopores offers further control over ionic transport. The aforementioned ion current rectification can for example be inverted by changing the negative charges on walls of a conical nanopores to positive charges. Introducing surface charge patterns with sharp junctions between zones of opposite surface charge creates an ionic diode, Figure 3.5.

In a diode, ion current in one direction is almost entirely suppressed forming the basis for the formation of an electric switch.

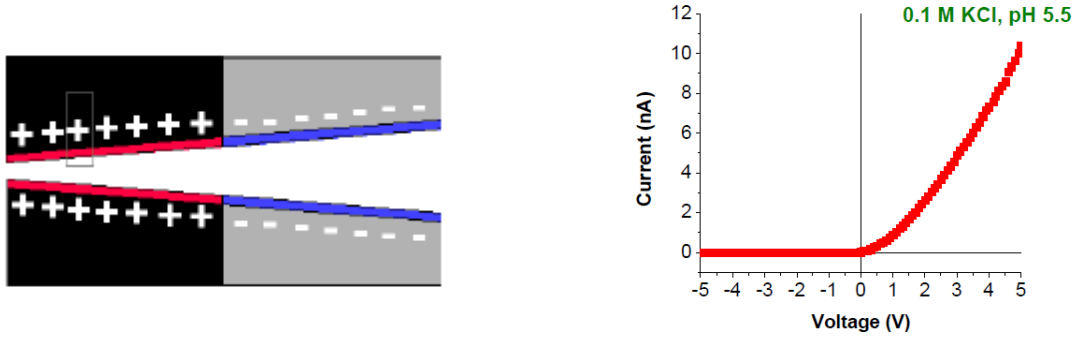

Figure 3.5: Left: Schematic of the charge patterns in an ionic diode nanopore. **Right:** I-V curve of the modified nanopore [5].

The zone with the negative surface charge is predominantly filled with positive ions, while the side with positive surface charge contains mostly negative ions, Figure 3.6. When a forward bias is applied, the negative ions are sourced from the positively charged region and the positive ions are sourced from the negatively charged region so that ion current can flow. This is the open state of the diode. By switching the voltage polarity a depletion zone is created, as there are no (or very few) negative ions to source from the negative side or positive ions from the positive side. Thus no current is allowed to flow, creating the off state of the system.

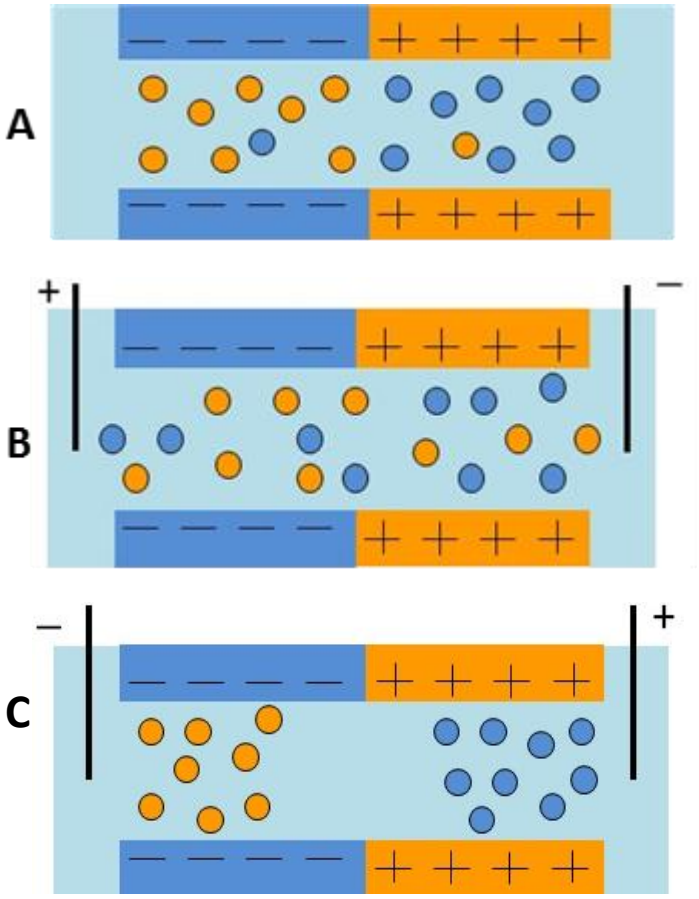

Figure 3.6: (A) Diode with zero bias applied. **(B)** Diode with a forward bias applied and flow of ion current. **(C)** Diode with reverse bias applied and the creation of a depletion zone thus there is no current flow.

3.3.2 Tuning Ionic Transport via Hydrophobic Interactions

Hydrophobic interactions provide yet another mechanism to control transport at the nanoscale. In contrast to electrostatic interactions, hydrophobicity controls transport of water and all species dissolved in it. There are three requirements in order for a pore to be classified as a gating hydrophobic nanopore. First the pore needs to be dewetted from the original wetted state, i.e. the water and ion transport needs to be halted. Dewetting involves removing liquid water from a portion of a pore. During this process the pore is partially or completely filled with water vapor, which halts the transmembrane transport. Dewetting is usually achieved through surface modification of the pore walls. The second requirement is wetting the dewetted pore. This is

achieved through the application of outside pressure or electric potential gradient, which forces the water vapor inside the pore to condense. Ions and water flow through the pore again, thus finite current is recorded. The final requirement is that after the removal of the critical pressure, the pore returns to a closed or dewetted state, once again halting the transport of water and ions through the pore.

The amount of pressure or voltage required to open the pore for transport depends on several factors including the pore opening diameter and the type of hydrophobic modification. An open nanopore, which exhibits hydrophobic gating, can subsequently become dewetted by removing the stimulus, repeating the whole process. Hydrophobic interactions at the nanoscale provide a natural mechanism for the preparation of a valve for water and all species dissolved in it. This will be discussed in more detail in the next sections as it is one of the two main focuses of this thesis.

3.3.3 Initial Dewetting and Wetting Nanopores

There are two important considerations for a pore to initially dewet, the surface properties of the pore walls and the opening diameter of the pore. First the surface of the pore must be hydrophobic, which is achieved through chemical modification of the pore walls. The nanopores used in this project originally have hydrophilic carboxyl groups on the walls to which long alkyl chains are attached via amide chemistry. In order to characterize the modification, a contact angle of a macroscopic polymer surface subjected to the same chemical modification as the nanopores was measured. Contact angles above 90° indicate a hydrophobic surface. The contact angle is measured by relating the difference between the surface-liquid tension, γ_{wl}, and the surface-vapor tension, γ_{wv}, with the surface tension of the liquid-vapor interface multiplied by the angle between them, Figure 3.7.

$$\gamma_{wl} - \gamma_{wv} = \gamma_{lv} Cos\,\theta \qquad [3.11]$$

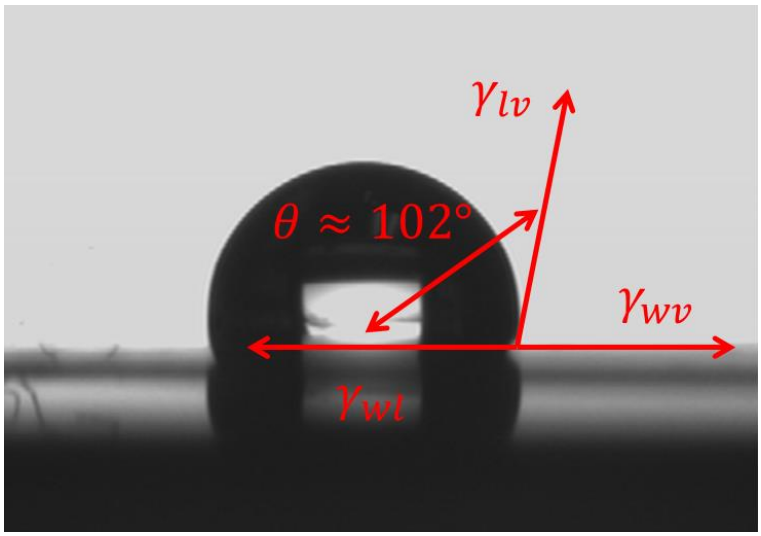

Figure 3.7: Drop of water on a surface modified with methyl esters for 24 hours. The contact angle of this surface is 102°.

The second important consideration in the initial dewetting is the separation distance of the hydrophobic surfaces. Neutron reflectivity measurements performed by Doshi, et al. indicated that the density of water close to hydrophobic surfaces is lower than the density of bulk water [18]. Modeling done by Luzar et al. predicts that when two hydrophobic surfaces are brought sufficiently close to each other, the liquid water in the region between the plates will undergo spontaneous evaporation. The upper limit of separation distance between two hydrophobic plates, D_c, is predicted by thermodynamic theory [19]. It is calculated by equating the grand potential of a confined vapor and the grand potential of a confined liquid, which gives a separation distance of

$$D_c = \frac{-2\gamma Cos\theta}{\rho\Delta\mu + {}^{b\gamma}/_{L}} \qquad [3.12]$$

In this equation γ is the surface tension, θ is the contact angle of the surface, ρ is the number density of the liquid, Δμ is the difference of the chemical potential of the bulk liquid and the liquid at the liquid gas interface, b is the geometry dependent constant on the order of unity, and L is the length of the surface. For a contact angle of 110° the predicted separation is 100 nm. This is much larger than the size of the nanopores studied in this thesis, which showed dewetting. The lower limit of this separation is predicted by kinetic theory and gives values around 1 nm. The spacing of the surfaces needs to be in between these values so that spontaneous evaporation of water can occur. Water in a nanopore will then be in a metastable state, Figure 3.8, making it allowable to change between a vapor and liquid state.

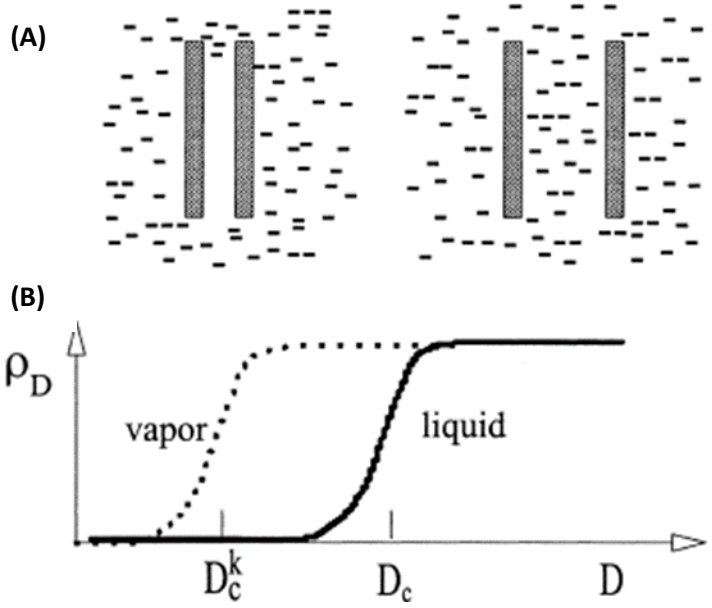

Figure 3.8: (A) Visual representation of the spacing needed for vapor and liquid states of water, respectively. **(B)** A graphical representation of the spacing required for liquid and vapor states. The vertical axis is the density of the liquid/vapor and the horizontal axis is the separation distance, with the kinetic and thermodynamic separations indicated [19].

3.3.4 Wetting a Hydrophobic Nanopore with Electric Field

The hydrophobic surfaces and small opening diameter prevent a hydrophobic nanopore from filling with condensed water. In order to wet the pore an outside stimulus e.g. in a form of pressure

difference needs to be applied. The required pressure difference to wet a hydrophobic nanopore can be estimated using the Young-Laplace equation:

$$P_{liquid} - P_{gas} = \Delta P = 2\gamma\kappa \qquad [3.13]$$

Where P denotes the pressure, γ is the surface tension and κ is the total curvature, which can be defined as:

$$\kappa = \frac{1}{r_1} + \frac{1}{r_2} \qquad [3.14]$$

with r_1 and r_2 as the radii of curvature. Since the liquid has a concave surface, the radii are defined as negative. Furthermore if the pore is sufficiently narrow then the curvature in the lateral plane, r_1, is equal to the radius of the pore opening and $r_2 = 0$. This simplifies the equation to:

$$\Delta P = \frac{4\,\gamma\,|Cos\,\theta|}{D} \qquad [3.15]$$

where D is the width of the channel. The equation predicts that the pressure required to wet a pore with a diameter of 10 nm whose walls are characterized with a contact angle of 102° is 59 atm. It would be therefore very challenging to build an experimental system which could be operated at such high pressures.

It was predicted theoretically however that instead of pressure difference, one can use electric field to fill a hydrophobic nanopore with condensed water [43]. Two groups provided experimental evidence that it is indeed possible. Smirnov, et al used electric field to wet silicon nitride (SiN) pores modified with SiH_{16} [23]. They proposed two models to explain the wetting of their nanopores, Figure 3.9. The first model suggests that the applied electric field forces the

meniscus on either side to bend inward, Figure 3.9A. When the meniscuses overlap the water and ions will be allowed to flow through the pore. The second model suggests that the applied electric field lowers the contact angle of the surface, known as electrowetting. This allows the meniscuses to move farther into the pore until the two meet and current is measured, Figure 3.9B. For electrowetting to be considered there needs to be a finite current at any applied voltage suggesting there is a continuous film of water along the whole pore length.

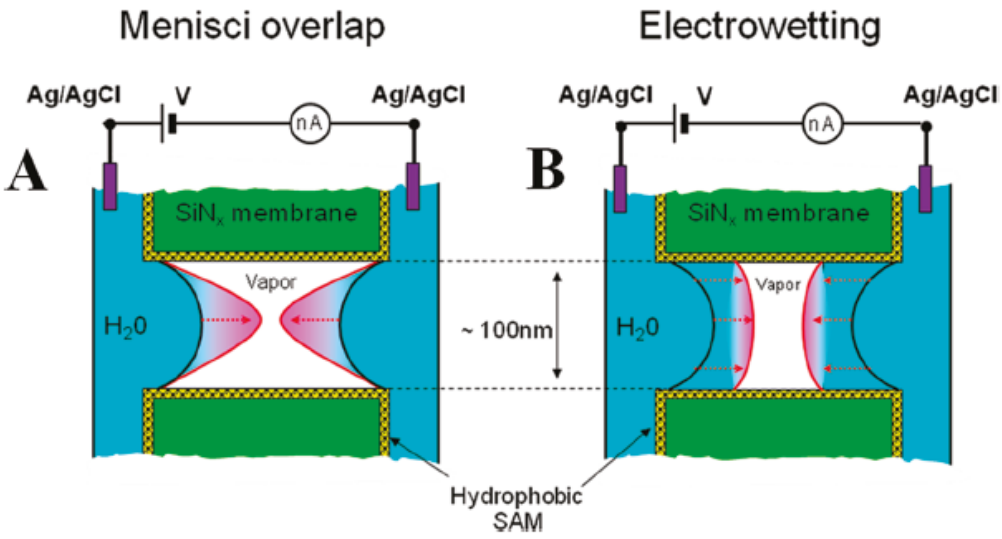

Figure 3.9: (A) Visualization of the menisci overlap model for the wetting of nanopores, where the menisci bend until meeting each other and allowing current to flow. **(B)** Visual representation of the electrowetting model. The contact angle of the surface is lowered due to the applied electric field allowing the menisci to move closer to one another, eventually touching and allowing current to flow [23].

Wetting hydrophobic nanopores with electric field was also reported by Powell et al [22]. These experiments were performed using single conically shaped PET nanopores with an opening diameter much smaller than these used by Smirnov et al. These experiments showed an existence of a complete off state suggesting that the electrowetting model cannot explain these results. It was a subject of this thesis to elucidate other mechanisms via which electric field opens a hydrophobic nanopore for water and ionic transport.

The electric field required to wet the hydrophobic nanopores was first estimated using the Young-Laplace equation with addition of the electrostatic pressure term:

$$\Delta P = \frac{4\gamma \cos\theta}{D} - \frac{\varepsilon_0}{2} E^2 \qquad [3.16]$$

where γ is surface tension of water, θ is the contact angle, D is the spacing of the surfaces or in this case the diameter of the nanopore, ε_0 is the permittivity of free space, and E is the electric field set by the applied voltage. The contact angle of C10 thiols on gold will be used to estimate the electric field required to wet the nanopore. A complete modification of the surface has a contact angle of 113° and the nanopore has a diameter of 6 nm and a length of 12 μm. However, equation 3.16 predicts the required field to be ~2.1×10^9 V/m thus much higher than applied experimentally. In order to explain experimental results on wetting hydrophobic nanopores we will present a model which takes into account the presence of residual surface charges.

3.4 Electroosmosis and Electrophoresis

When describing ion transport through nanopores, the Navier-Stokes equations are frequently neglected since the velocity of solution in nanopores is often very low. However the velocity of the solution in micropores is significant and needs to be considered. There are two electric field induced transport phenomena in micropores which are important for the results presented in the thesis: elecotroosmosis and electrophoresis. Electroosmosis is the flow of the solution caused by movement of ions in the electrical double layer thus it occurs in the direction of counterions transport. Electroosmotic and electrophoretic transport will be first treated separately and then combined to facilitate a better understanding of the transport of particles in a micropore.

As previously discussed an electrical double layer (EDL) forms on a charged surface where the potential is given by Equation 3.1. Electroosmotic flow occurs when an electric field has a component that is applied parallel to the charged surface. The applied electric field causes the ions in the diffuse layer of the EDL to flow. The EDL drags the fluid with it creating a net flow. When the Debye length is much smaller than the pore, a plug-like flow develops, Figure 3.10. The velocity of the fluid due to electroosmosis is determined by the Navier Stokes equation, Eq. 3.8. In addition to the initial assumptions made above, we will also assume that there is no applied pressure. Furthermore we will assume that the fluid flow is only along the pore axis. This allows for the Navier Stokes equation to be written as follows

$$0 \cong \nu \frac{\partial^2 u(r)}{\partial r^2} + \rho E_{ext} \qquad [3.17]$$

where ρ is the charge density as described by the Poisson equation and E_{ext} is the externally applied electric field. Inserting ρ and using the boundary conditions that the velocity of the fluid is zero at the walls ($u(\pm a) = 0$) and the potential of the pore walls is given by the screened surface potential of the pore walls i.e. the zeta potential, (($\phi(\pm a) = \zeta_s$), the electroosmotic fluid velocity is given as

$$u_{eo} = \frac{\varepsilon_0 \varepsilon_r E_{ext}}{\upsilon} (\phi_s(r) - \zeta_s) \quad [3.18]$$

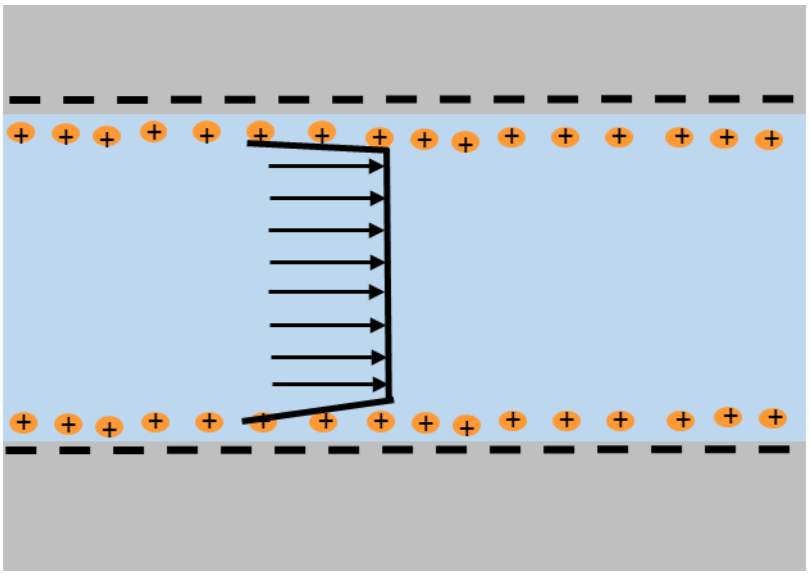

Figure 3.10: A visual representation of plug-like electroosmotic flow in a charged cylindrical channel.

The other form of transport through the pore is by electrophoresis. Electrophoresis is the movement of a charged species such as ion or particle relative to the bulk fluid. Calculating the velocity of electrophoretic flow is performed in a similar manner to the electroosmotic flow, except the coordinate system will be changed such that it is fixed on the particle. The velocity of the fluid far from the particle can be assumed to be constant and negative. Using $\phi_p(r)$ as the potential due to the surface charge of the particle at a distance r from the particle, the boundary conditions are as following: $\phi_p(0) = \zeta_p$, $u(0) = 0$, and $\phi_p(\infty) = 0$. Repeating what was done above for electroosmosis with the new boundary conditions gives an electrophoretic velocity of

$$u_{ep} = \frac{\varepsilon_0 \varepsilon_r E_{ext}}{\upsilon} \left(\phi_p(r) - \zeta_p\right) \quad [3.19]$$

Both of these flows are present in the pore at the same time. Thus particle transport through the pore is determined by a competition of these flows. In order to combine these two velocities the coordinates of electrophoretic flow velocity need to be switched to match the coordinate system

of electroosmotic flow velocity. For a detailed derivation of the addition of these two velocities the reader to referred to the dissertation of M. Pevarnik [44]. The result gives

$$u = u_{eo} + u_{ep} = \frac{\varepsilon_0 \varepsilon_r E_{ext}}{\upsilon}\left(\zeta_s - \zeta_p\right) \qquad [3.20]$$

This shows that the zeta potential of the surface and the particle are important for determining the transport of particles through the pore. Thus a particle with a high zeta potential relative to the zeta potential of the pore walls will be transported through the pore by electrophoresis, while a particle with a lower zeta potential will be transported through the pore by electroosmosis.

Chapter 4

Hydrophobic Conical Nanopores Results and Discussion

The transport properties of hydrophobic nanopores were recorded in the same conductivity cells they were etched and modified in. All pores used had small opening diameters between 5 and 12 nm and large opening diameters between 300 and 700 nm. Current-voltage curves were measured in 10 mM, 100 mM, and 1 M KCl pH 8 using a Keithly 6487 picoammeter/voltage source with Ag/AgCl electrodes. Voltages were swept from -10 V to +10 V with 100 mV steps and 3 second pauses to reduce capacitance. A few measurements were taken with an Axopatch 200B and a 1322A Digidata (Molecular Devices) where voltages were swept from 0 V to +10 V, +10 V to 0 V, 0 V to -10 V, and then -10 V back to 0 V. Each voltage was recorded for 30 seconds. The working electrode was placed in the reservoir with the large opening and the ground electrode was placed in the reservoir with the small opening for all scans.

4.1 Results with Propylamine, Hexylamine, and Decylamine Modified Nanopores

Single conically shaped nanopores in polyethylene terephthalate (PET) were modified with propylamine, hexylamine, and decylamine in order to understand the effect of alkyl chain length on hydrophobic gating. Increasing the carbon chain length increases the hydrophobic character of the molecules. In order to quantify the hydrophobicity of the modified surfaces, the contact angles of modified PET foils without nanopores were measured. It could be expected that the decylamine modified surface would have the highest contact angle followed by hexylamine, propylamine and the unmodified PET surface the lowest. While the unmodified PET was characterized with the lowest contact angle of 58°, the PET surfaces that were modified with the amines all had similar contact angles of ~77°, Figure 2.6. Values of contact angle below 90° suggest that the surfaces may not have been completely modified, which is in agreement with previous observations on the difficulty of achieving full conversion of carboxyl groups with EDC [45]. Thus the measured

contact angle represents a composite surface, containing regions with hydrophobic amines and regions with the hydrophilic carboxyl groups. Another indication for the existence of unreacted carboxyl groups is the ion current rectification exhibited by the modified nanopores. Rectification of ion current in conically shaped nanopores occurs only when the pore walls are charged.

All pores modified with one of these three different alkyl chains exhibited hydrophobic gating, albeit at different voltages and salt concentrations. Two nanopores were modified with propylamine and they both showed similar KCl concentration dependence of the transport properties. The modified 5 nm pore exhibited very little ionic conductance in 10 mM KCl; the 10 V current-voltage scan had weak hydrophobic gating with the closed state below 5 pA and the open state reaching ~ 10 pA, Figure 4.1A. In 100 mM KCl the pore was open for ionic transport for all voltages, but the ion current values were significantly lower than before propylamine attachment. In 1 M KCl the pore continued to conduct ion current for all studied voltages and the values of the current were very similar to these seen before modification. Recordings in 10 mM KCl were subsequently performed again in attempt to return the pore to a gating state, however the pore remained open for ionic conductance. Only after allowing the pore to air dry did the pore close for transport and exhibited gating in 10 mM KCl.

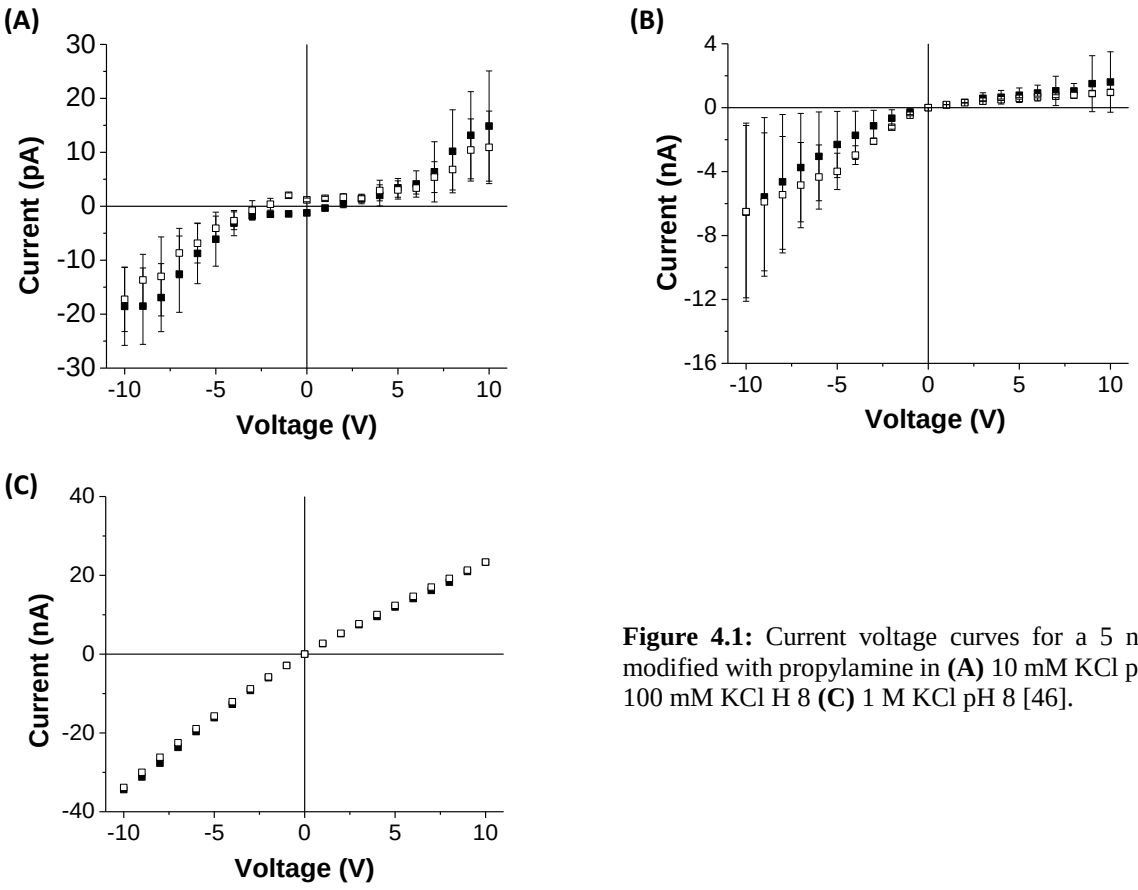

Figure 4.1: Current voltage curves for a 5 nm pore modified with propylamine in **(A)** 10 mM KCl pH 8 **(B)** 100 mM KCl H 8 **(C)** 1 M KCl pH 8 [46].

Two pores modified with hexylamine also exhibited hydrophobic gating. The 6 nm pore was mostly non-conductive in 10 mM KCl with current values similar to what was seen in the propylamine modified pores, Figure 4.2A. The pore did gate in 10 mM KCl opening around 9 V for positive voltages and around 3V for negative voltages. Comparing this to the propylamine modified pore, the opening/closing values for the negative voltages are very similar. However the positive opening/closing voltages are larger for the hexylamine modified pore. In 100 mM KCl the pore initially switched between conducting and non-conducting states and eventually opened for all voltages. The inset in Figure 4.2B shows the hydrophobic gating behavior of the nanopore at lower voltages. In 1 M KCl the pore was conductive for all voltages and exhibited rectification

of the ion current, with the inset in Figure 4.2C showing that the nanopore is indeed open for lower voltages.

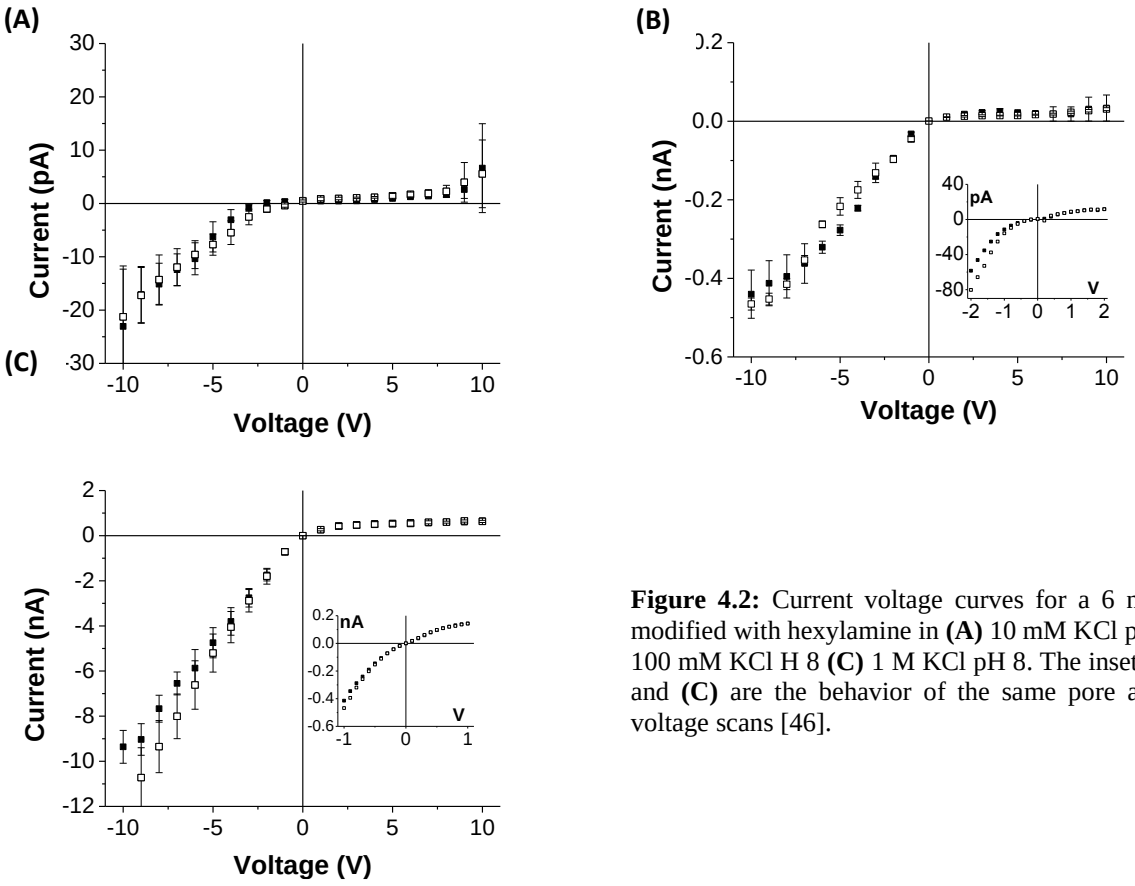

Figure 4.2: Current voltage curves for a 6 nm pore modified with hexylamine in **(A)** 10 mM KCl pH 8 **(B)** 100 mM KCl H 8 **(C)** 1 M KCl pH 8. The insets in **(B)** and **(C)** are the behavior of the same pore at lower voltage scans [46].

The largest number of nanopores was modified with decylamine, 19 in total. Seven of them were closed for ionic transport in all molarities and for all voltages. Five pores were open for all concentrations and voltages. This is most likely due to the fact that the modification did not occur in the narrowest region of the pore where the vapor formation would create the largest effect on the ion current. The remaining seven pores were closed in 10 mM KCl and gated (i.e. switched between conducting and non-conducting states) in either 100 mM KCl or in 1 M KCl. The 9 nm pore shown in Figure 4.3 was closed in 10 mM KCl for all voltages. In 100 mM KCl the pore did not conduct ionic current up to 8 V and opened for ionic current only on the return sweep. For

subsequent voltage sweeps the pore gated with opening voltages around +4 V and -5 V. Current-voltage curves recorded in 1 M KCl showed repeated gating with threshold voltage values of ~1.5 V; 26 scans were performed for this nanopore, of which there is a summary of the opening and closing voltages in Figure 4.5.

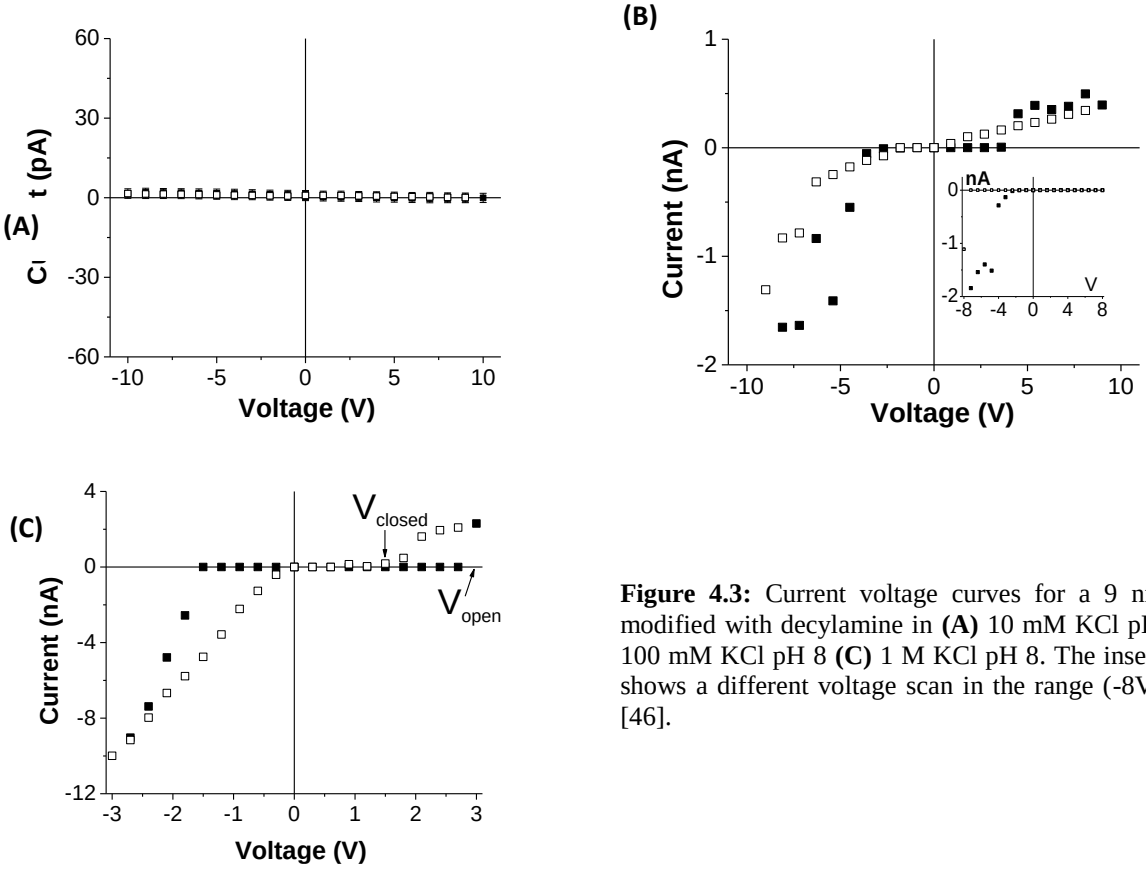

Figure 4.3: Current voltage curves for a 9 nm pore modified with decylamine in **(A)** 10 mM KCl pH 8 **(B)** 100 mM KCl pH 8 **(C)** 1 M KCl pH 8. The inset in **(B)** shows a different voltage scan in the range (-8V, +8V) [46].

4.2 Unique Behaviors of the Decylamine Modified Pores

The decylamine modified pores exhibited two types of behavior that were not seen in the propylamine or the hexylamine modified pores. First, current-voltage curves of these pores revealed existence of hysteresis i.e. the voltage required to open the pore and allow ions to flow was larger than the voltage at which the pore dewetted and halted the transport of ions, Figure 4.4.

For the hysteresis in Figure 4.4, the voltage required to open the pore is 7 V and the voltage that this pore closed at is 1.5V.

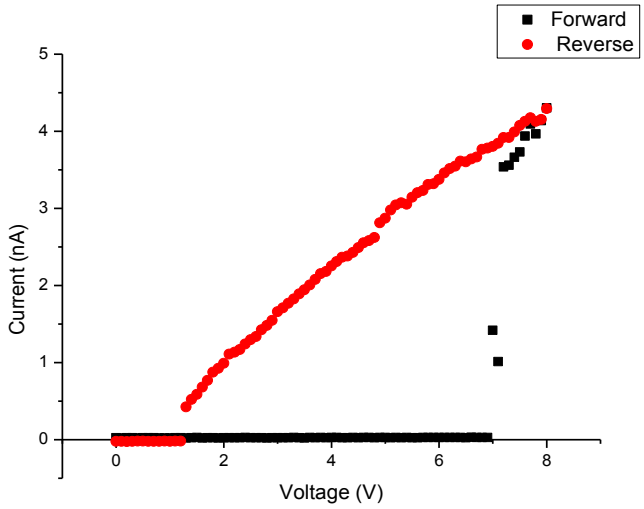

Figure 4.4: Example of hysteresis in the 7 nm pore modified with decylamine. The pore required to open the pore and did not close again until 1.1 V [47].

The other unique feature of the decylamine modified pores was the ability to repeatedly switch between open/conducting and closed/non-conducting states. This behavior was seen in two other pores in addition to the one discussed in detail above. These pores had opening diameters of 9, 7 and 6 nm. In 20 out of 26 scans performed on the 9 nm pore in 1 M KCl pH 8, a clear switch between conducting and non-conducting states was observed, typically at ~1 V, Figure 4.5A. The pore with the most reproducible gating behavior had the opening diameter of 6 nm and was subjected to 50 voltage scans in 1 M KCl pH 8, (Figure 4.5C). An average of 30 scans shown in Figure 4.5D suggests that throughout the scans, the voltages required to open or close the pore for ionic transport remained nearly constant.

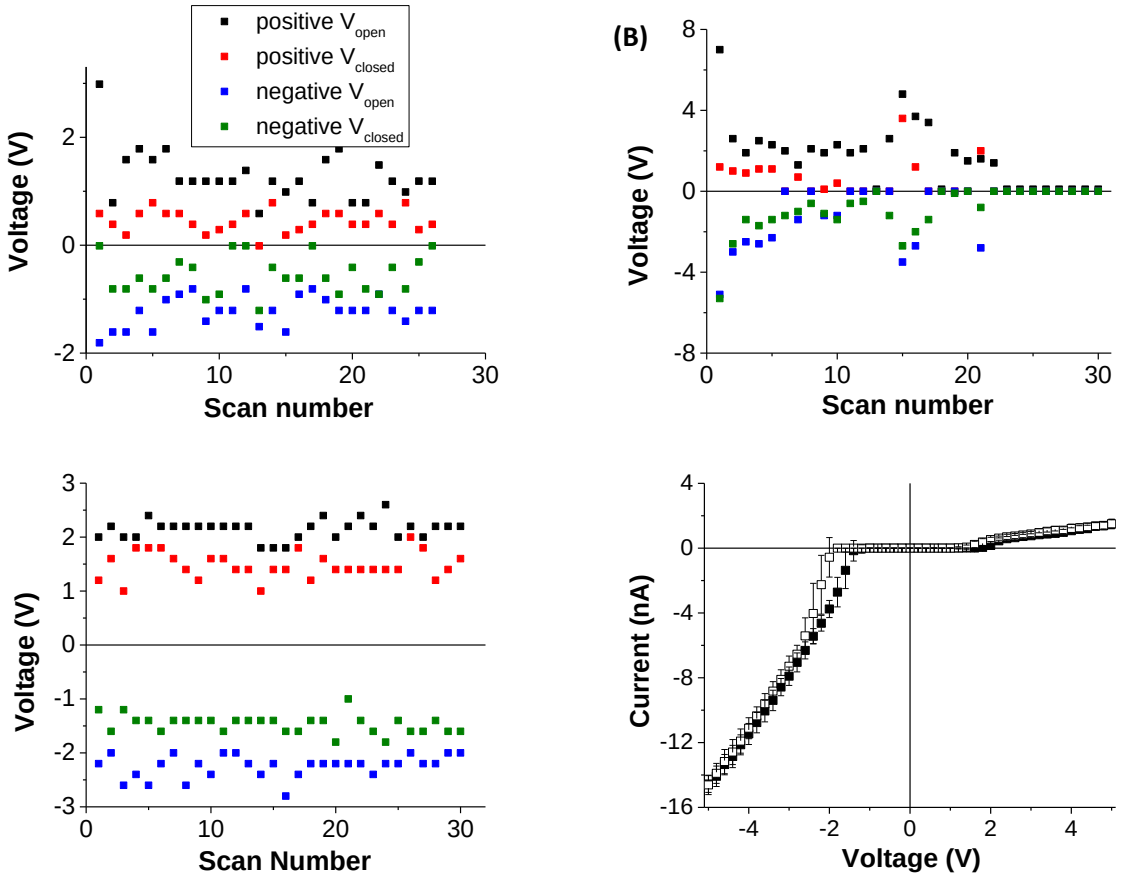

Figure 4.5: Scatter plots of the of the opening and closing voltages versus scan number for the **(A)** 9 nm pore **(B)** 7 nm pore **(C)** 6 nm. **(D)** Average of 30 scans of the 6nm pore In (C) I would mark V_{open} and V_{closed} [46].

4.3 Discussion of Results

The experimental results obtained with nanopores that were modified with alkyl chains revealed that salt concentration is another parameter which modifies hydrophobic interactions at the nanoscale. The importance of an electrolyte for hydrophobic gating was predicted theoretically but never shown experimentally. L. Liu et al preformed molecular dynamic simulations of hydrophobic pores showing that higher pressures are required for salt solutions to wet the pore over pure water, indicating that the presence of ions inhibits wetting [48]. However the opposite effect, ions promoting wetting, has been predicted as well. Dzubiella et al. have shown that the

addition of ions into the solution promoted wetting as the electric field acting on the ion lowers the potential barrier by a few k_bT [49]. Further simulations have shown that the charge density of ions modulate the hydrophobic interactions between two parallel plates, where high charge density ions promote dewetting and lower charge density ions promote wetting [50].

Our experiments also suggested that the walls of the examined pores were chemically heterogeneous and consisted of hydrophobic and hydrophilic islands. We anticipate that the vapor regions will form at the hydrophobic zones. Assuming there is a single vapor pocket in the pore, the required pressure to condense the water vapor and open the pore for transport can be recalculated using the Young-Laplace with the electrostatic pressure term:

$$\Delta P = \frac{4\gamma \cos\theta}{D} - \frac{\varepsilon_0}{2} E^2 \qquad [4.1]$$

If the pore contains one 20 nm long vapor pocket, and the pore opening diameter is 6 nm, eq. (4.1) predicts that the magnitude of voltage needed to wet the pore is 40 V. The required voltage would be even higher if there were multiple vapor pockets inside the pore. Since our hydrophobic nanopores opened for ionic transport at much lower voltages, we predicted another source of pressure difference had to be considered.

Smirnov et al used an electrowetting model to explain the electric field induced wetting of their hydrophobic nanopores [23]. In order to use the electrowetting model, the closed state of the system would have to be characterized with a finite conductance, indicating the nanopore is connected electrically throughout the whole length. All the nanopores examined in this set of experiments were characterized by a modification-independent closed state of just a few pA. Moreover, electrowetting as described in Smirnov et al does not predict salt dependence of the hydrophobic gating.

In order to explain the effect of the electrolyte on the process of wetting and dewetting, the contribution of the residual surface charge on the pore walls will be examined. To simplify the system, we will consider a nanoslit composed of two charged parallel plates separated by a few nm, Figure 4.6, and follow the model developed by J. Lee et al [51]. Assuming there is no fluid flow or gravity effects, the stress on the meniscus can be described as the sum of the osmotic pressure, Π, and the Maxwell stress.

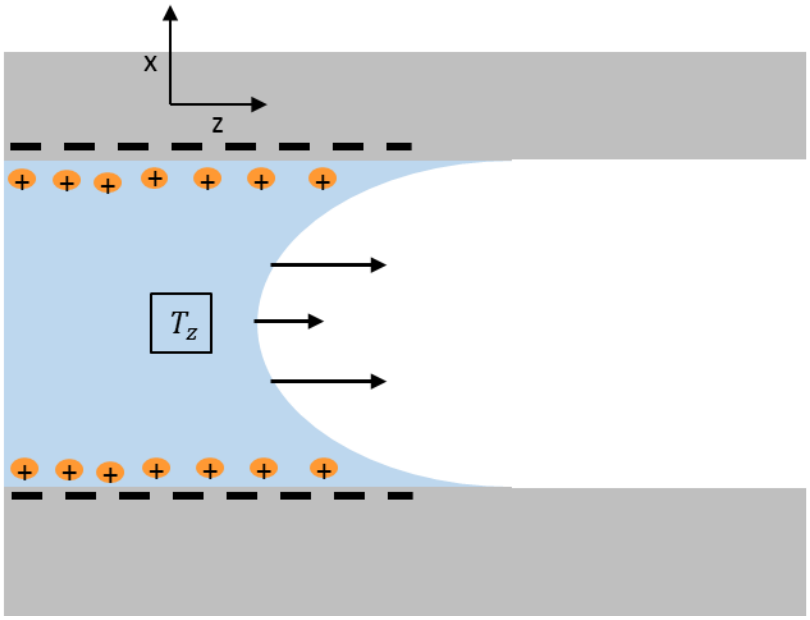

Figure 4.6: A schematic of the liquid vapor interface inside of a nanoslit where T_z acts on the interface.

The model by J. Lee is based on electrostatics thus no external field is applied. The nanoslit allows for the assumption that the electric field produced from the charges on the surface is only in the x-direction (Figure 4.6). The total stress on the liquid vapor interface perpendicular to the slit axis is given by:

$$T_{zz} = \Pi + \frac{\varepsilon\,\varepsilon_0}{2} E^2 \qquad [4.2]$$

The electric field, *E*, in equation 4.2 is anisotropic i.e. dependent on the x position, as predicted by the Poisson-Bolztmann equations. This anisotropy causes the deformation of the liquid vapor interface and gives the basis for electrocapillarity effect. The osmotic pressure is calculated with the local electric field, E, and the free charge density, n_f, and fulfills the Gauss equation. The free charge density is determined by the difference between the concentration of counter-ions and co-ions.

$$\nabla \Pi = n_f E \qquad [4.3]$$

The electric field is calculated from the electric potential produced from the charges on the surface. Thus the regions filled with salt solution are comprised of mainly counter ions. The concentration and electric potential is described by the Poisson-Boltzmann equation, which can be linearized for the low surface potential limit:

$$\psi'' = k^2\psi, \;\; k = \frac{2z^2e^2n_b}{\varepsilon\varepsilon_0 k_b T} \qquad [4.4]$$

where ψ is the electric potential, k is the inverse Debye length, n_b is the number density of ions, and k_B is the Boltzmann constant. The solution satisfies the $\psi'(0) = 0$ and $\psi(h)$ = V boundary conditions giving:

$$\psi(r) = V\frac{\cosh kr}{\cosh kh} \qquad [4.5]$$

The electric potential has a radial profile that leads to a non-homogenous electric field.

$$E(r) = -\psi'(r) = -Vk\frac{\sinh kr}{\cosh kh} \quad [4.6]$$

Therefore the osmotic contribution is the outward stress at the centerline is:

$$\Pi(0) = 2n_b k_b T + n_b k_b T \left(\frac{zeV}{k_b T}\right)^2 \frac{1}{(\cosh kh)^2} \quad [4.7]$$

Thus by substituting the osmotic contribution and the calculated electric field the total outward stress on the liquid vapor interface is given as:

$$T_z = n_b k_b T \left(\frac{zeV}{k_b T}\right)^2 \frac{2\cosh 2kr}{\cosh 2kr+1} + 2n_b k_b T \quad [4.8a]$$

$$V = \frac{\sigma}{k\varepsilon\varepsilon_0}\frac{\cosh kh}{\sinh kh} \quad [4.8b]$$

Figure 4.7 shows a graph of the total pressure and the Maxwell stress term on the liquid-vapor interface for different salt concentrations with T = 293 K, h = 3 nm, and σ = 0.02 C m^{-2}. The calculations predict that the total pressure reached tens of atm and indeed increase with the increase of salt concentration. The results also indicate that both Maxwell stress and the osmotic components need to be considered in order to correctly predict the salt dependence on hydrophobic gating. The calculations also explain why in some nanopores, a mere change of electrolyte concentration led to the nanopore wetting. The future studies will be focused on solving the equation for a cylindrical geometry and adding an external electric field.

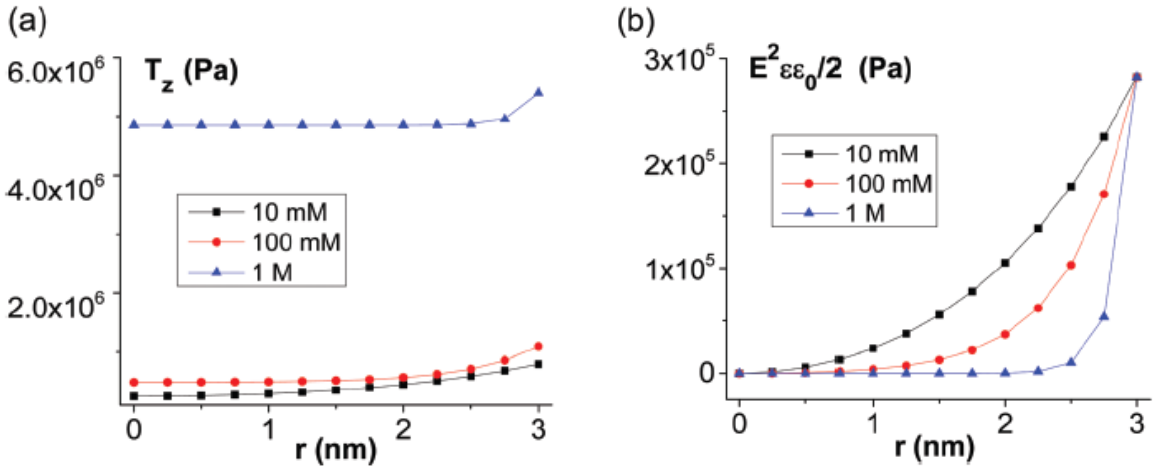

Figure 4.7: The outward stress on the liquid vapor interface calculated with a separation distance of 2r. On the horizontal axis 0 corresponds to the center of the nanoslit. (a) The total pressure, Eq 4.9, on the liquid vapor inteface in the nanoslit. (b) Maxwell stress contribution on the liquid vapor interface [46].

Chapter 5

Resistive Pulse Technique for Measuring Physical Characteristics of Particles and Cells

The resistive-pulse technique is used to size and count nano to micro sized objects, such as single molecules of DNA and proteins, viruses, particles, and biological cells. This is the method utilized by the Coulter Counter to perform a blood count in doctor's offices and hospitals. A smooth cylindrical channel is placed between two reservoirs of a conductivity cell, and a voltage and pressure difference are applied causing an ion current and fluid to flow, Figure 5.1. When an object enters the channel it occludes the pore, resulting in an increase in the measured resistance, and consequently a decrease in the measured current. This change of resistance can be used to calculate the volume of the object if the pore opening diameter is known [52]:

$$R_{particle} - R_{empty} = \frac{4\rho d^3}{\pi D^4} S\left[\frac{d}{D}\right] \qquad [5.1]$$

$$S\left[\frac{d}{D}\right] = \left[1 - 0.8\left(\frac{d}{D}\right)^3\right]^{-1}$$

$R_{particle}$ is the resistance of the system when the particle is in the channel, R_{empty} is the resistance of the channel with only salt solution, ρ is the resistivity of the fluid, d is the diameter of the translocated object, D is the diameter of the channel, and $S\left[\frac{d}{D}\right]$ is the shape factor. The shape factor is a term used to describe how the object modulates the electric field inside the channel. The shape factor is especially important when the size of the passing objects approaches the size of the pore opening. For the experiments discussed below it is more convenient to use the normalized change of the baseline current to compare pulses created by individual particles of different sizes. Turning

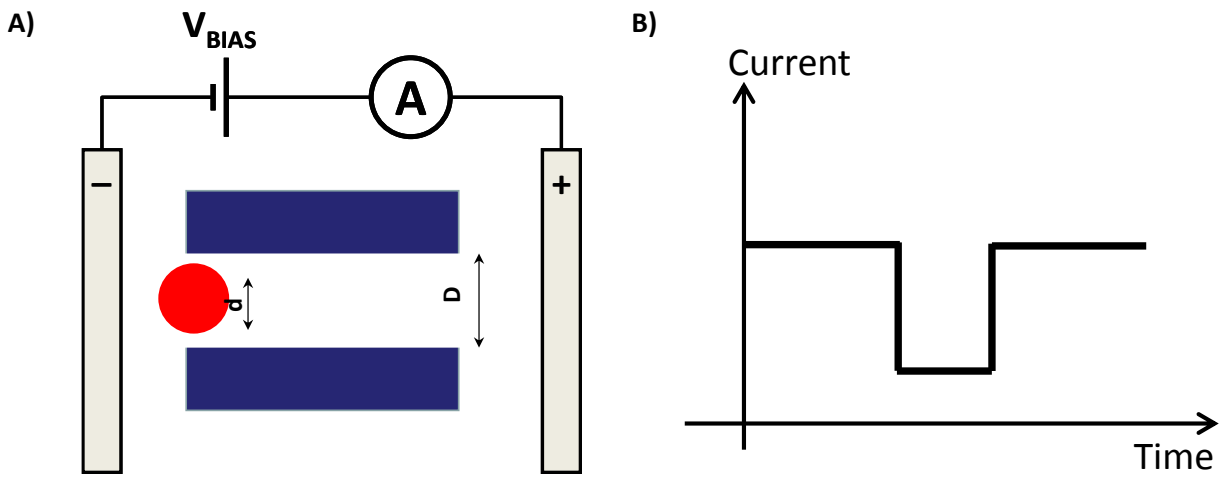

Figure 5.1: A) Setup of a resistive-pulse experiment and visual representation of a particle translocation. **B)** Example of a resistive pulse event in a smooth channel.

normalized resistance into normalized current is based on the ohmic relationship of current with voltage, V:

$$\frac{R_{particle}-R_{empty}}{R_{empty}} = \frac{\frac{V}{I_{particle}} - \frac{V}{I_{empty}}}{\frac{V}{I_{empty}}}$$

$$= \frac{I_{empty}-I_{particle}}{I_{particle}} \qquad [5.2]$$

where $I_{particle}$ and I_{empty} are currents with and without the particle in the pore, respectively.

The majority of resistive-pulse experiments are performed with smooth cylindrically shaped pores. Our group however has postulated that adding roughness to the channel walls allows for multi-pronged characterization of passing objects beyond sizing. The notion of roughness used here indicates that the diameter of a pore varies along the pore axis. Polyethylene terephthalate (PET) pores prepared by the track-etching technique and used in the experiments are characterized by significant roughness resulting from their semi-crystalline as well as laminar structure. The pores are prepared by several hours of etching at an elevated temperature, which leads to over-

etching of the regions between the strata and formation of large local cavities. 3D topography of the pores can be visualized via preparation of their metal replica. Resistive-pulses of particles through the pores offer an independent and non-destructive method to learn about the pore structure. We have shown that fluid transport through such rough channels is non-trivial and leads to the formation of local pressure differences along the pore axis, even in cases when no pressure difference is applied macroscopically. We hypothesized that these local pressure differences will lead to transient object deformation, which can be used to elucidate the object's mechanical properties. Rough pores also allow for the determination of the object shape's [53], but this aspect will not be discussed here.

5.1 Previous Resistive Pulse Experiments: Tracing Pore Topography, Sizing and Detection from Concentrated Solutions.

Figure 5.2 shows ion current through a single pore with an average opening diameter of 870 nm recorded in the presence of 220, 330 and 410 nm spherical carboxylated polystyrene particles. The experiment was performed in a conductivity cell whose one reservoir was filled with

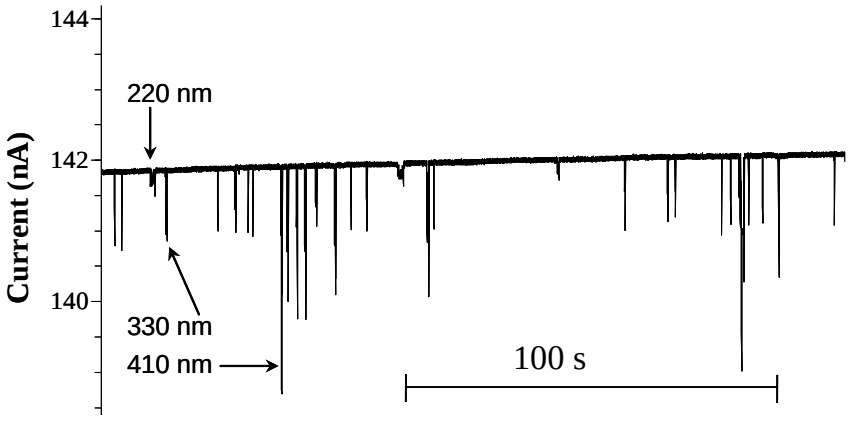

Figure 5.2: Ion current versus time recording of an 870 nm pore with 220, 330, and 410 nm particles in 1 M KCl pH 8 with 0.1% Tween 80. Each particle size has a concentration of ~$2 \cdot 10^9$ particles/mL. A single transient drop in current corresponds to a single particle translocating through the pore. Transolcations of 220, 330, and 410 nm particles are indicated [54].

1 M KCl solution containing the particles, while the other reservoir was filled only with the salt solution. Voltage was applied across the membrane and the particles transported in the direction of electrophoresis, so that they moved towards a positively biased electrode. When investigating the shape of the pulses in detail, it was discovered the pulses had a complex structure featuring a series of peaks and valleys. When a particle passes through a region with a larger local diameter it blocks the current to a smaller extent than when passing through a narrower region, Figure 5.3A. Since the pulse structure given by each different particle size was very similar, it was concluded that the pulses reflect the pore 3D topography.

It was also confirmed that in spite of the roughness, the pores can still be used for particle sizing, such that the recorded ΔI/I was correlated with the object volume, Figure 5.3.B. Traditional resistive pulse experiments with smooth channels require performing analysis from dilute solutions

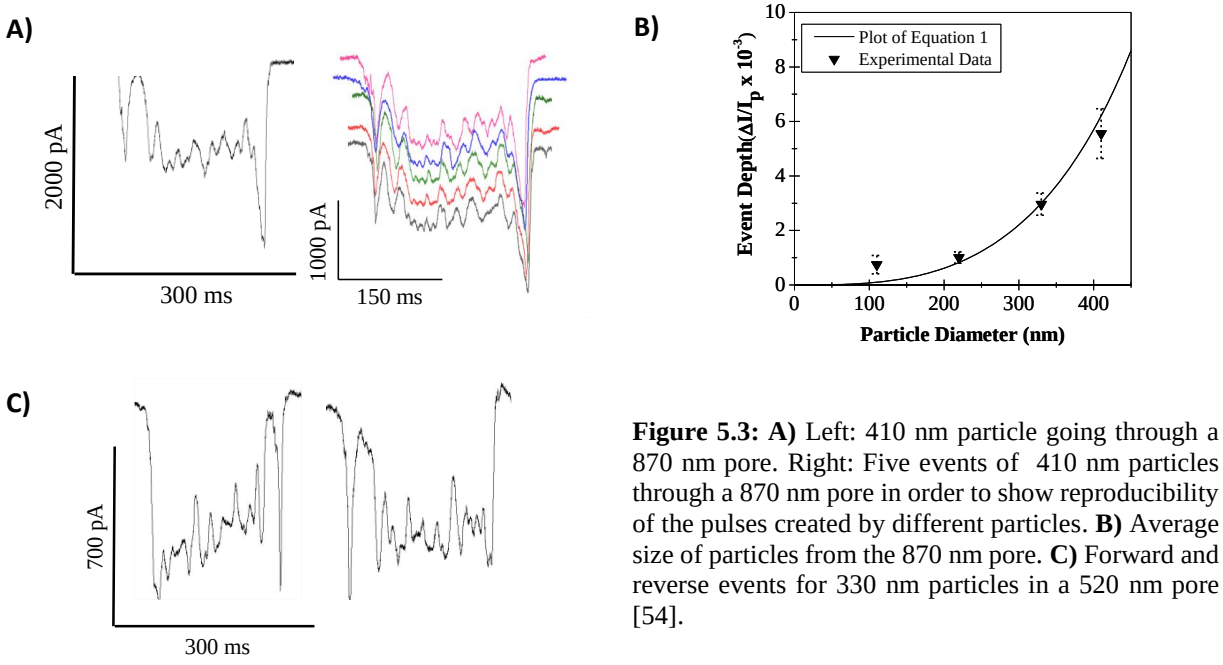

Figure 5.3: A) Left: 410 nm particle going through a 870 nm pore. Right: Five events of 410 nm particles through a 870 nm pore in order to show reproducibility of the pulses created by different particles. **B)** Average size of particles from the 870 nm pore. **C)** Forward and reverse events for 330 nm particles in a 520 nm pore [54].

so that the probability of two particles residing in a pore at the same time is negligible. It is because a smooth pore cannot differentiate between two smaller particles and one larger particle of equal

volume. Roughness allows for particle detection and characterization from concentrated solutions, so that examined samples do not need to be diluted for accurate results, Figure 5.4. An ability to perform analysis from concentrated solutions is especially important when detecting objects which are rare or present in an unknown concentration, such as circulating tumor cells (CTCs) in blood. The detection from a concentrated solution can be achieved since passage of each particle causes a unique set of ion current modulations. If a second particle enters the pore while the first one has not exited yet, the event shape of the second particle will be simply superimposed on the pulse of the first one. The uniqueness of the events also allow for the detection of where and how long particles get stuck, Figure 5.4B.

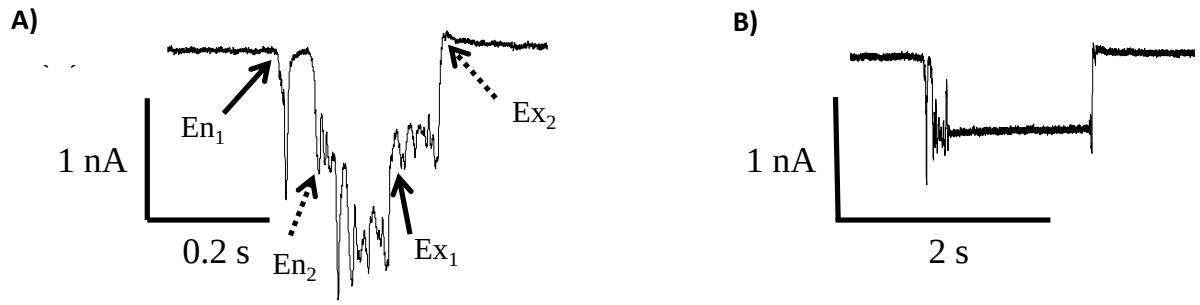

Figure 5.4: A) Two particle event in a 520 nm pore **B)** A stuck particle in a 520nm pore seen as an interruption of ion current pulse shape [54].

5.2 Velocity Profiles and Pressure Gradients in Rough Pores

Particles passing through a pore with surface charges on the pore walls will be transported by the effects of electroosmosis or electrophoresis. In case of negatively charged particles passing through a negatively charged pore, electrophoretic and electroosmotic transport occur in opposite directions. A particle will move in the direction of electrophoresis if the surface charge density of

the particle is higher than the surface charge density of the pore. Less charged and uncharged particles will move in the direction determined by electroosmosis.

It is also expected that the recorded resistive pulses are intimately related not only with the topography of the pore but also local fluid velocities. In order to understand in greater detail how pore roughness influences detection of particles, a series of pores differing in diameter, aspect ratio and roughness were prepared and used for the detection of particles. The results were then applied to a series of biological cell trials.

5.2.1 Initial Experiments: Particles and Mouse Cells

Particle experiments were performed in either 100 mM or 10 mM KCl. The average pore diameters ranged from 1 μm to 15 μm. The pore length varied between 11 μm and 35 μm. Measurements were performed using the commercial amplifier Axopatch 200B (Molecular Devices, Inc) in cases when the recorded current did not exceed 200 nA (the upper limit of the system). The amplifier could be therefore used for experiments in 100 mM KCl with pores whose diameter was less than 1.5 μm as well as in 10 mM KCl for pores with diameters below 4 μm. Ion currents through larger pores were measured using a custom CMOS chip based potentiostat as it is capable of measure μA of current with sub nA precision [55]. Two types of particles were used, negatively charged carboxylated polystyrene particles which ranged in diameter from 410 nm to 5 μm and neutral poly(methyl methacrylate), PMMA, particles with a diameter of 400 nm. The concentration of the particles in solution was approximately $2 \cdot 10^9$/mL. All solutions contained 0.1% Tween 80 as the surfactant was found very effective in preventing the particles' aggregation [54]. In all performed experiments, positive voltages were correlated with electroosmotic flow and negative voltages are correlated with electrophoretic flow.

Figure 5.5 shows a 3 μm pore that transported particles 1 μm in diameter both electroosmotically and electrophoretically. The pulse shape for both events consisted of a negative peak (current below the baseline) and a positive peak (current about the baseline level), however, the order of these peaks is different for particles transported by electrophoresis versus particles transported by electroosmosis, Figure 5.5. Double peak events are caused by the transient modulation of the ionic concentration at the entrance and exit of the pore [56]. The events with particles transported electrophoretically were comprised of a current decrease followed by a current increase. The current increase is caused by excess positive ions carried through the pore by the negatively charged particle and the increased concentration of the ions at the pore exit from where they are sourced. This increase in positive ions at the pore exit is also due to concentration polarization. Meanwhile, the pulses of particles transported electroosmotically started with the current increase, because the particles travelled through the pore for the opposite voltage polarity; the increase of cation concentrations occurs therefore at the pore entrance.

Calculation of the particles' sizes using their relative current change elucidated another difference between the particles transported by electroosmosis and those transported by electrophoresis. The particles transported in the direction of electrophoresis sized to around 1 μm, which is close to the value given by the manufacturer (Bangs Labs). The particles that were transported in the direction of electroosmosis sized to about 1.5 μm. Sizing with the resistive pulse method is voltage independent, suggesting that the larger particles are transported electroosmotically because they have a lower surface charge density. The large dispersion of the particles' size was confirmed by light scattering and SEM.

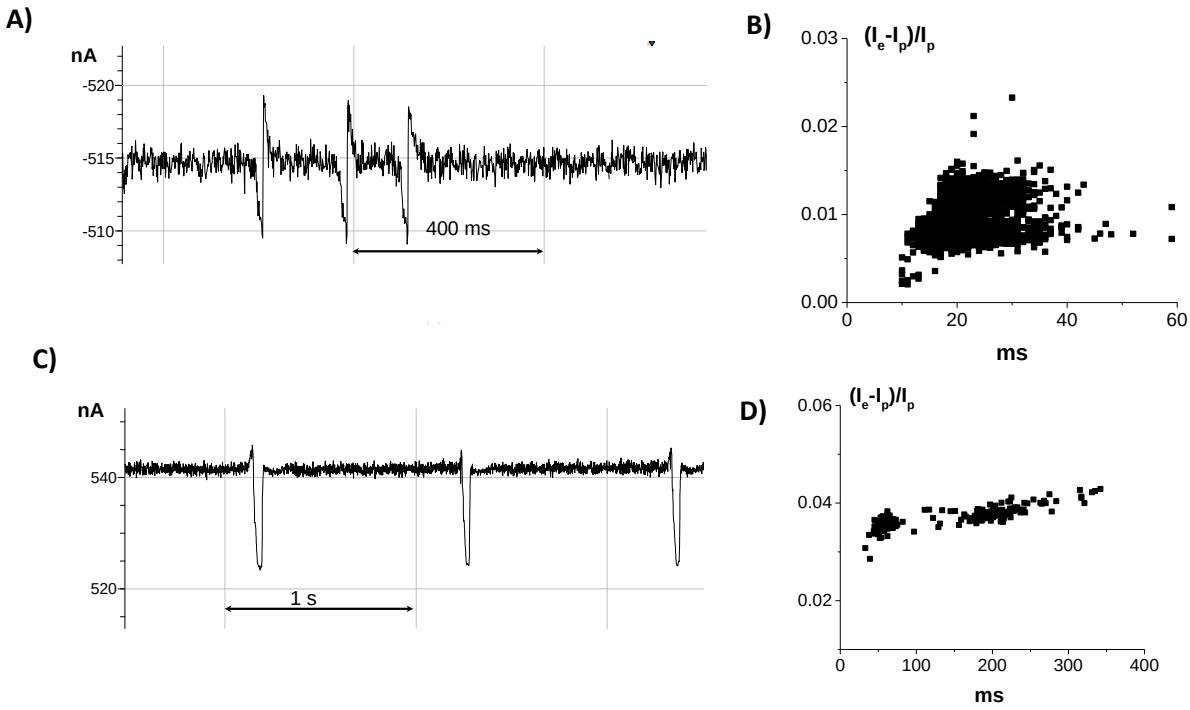

Figure 5.5: Recordings of ion current for 1 µm particles passing through a 3 µm in diameter pore of length of 9 µm. Example pulses of particles that passed through the pore in the direction of (**A**) electrophoresis and (**B)** electroosmosis **(C)** Scatter plot of relative current change versus event duration for electrophoretically transported particles. **(D)** Scatter plot of relative current change versus event duration for electroosmotically transported particles [39].

Scatter plots of the relative current change against the event duration show that particles transported by electroosmosis have more variability in their event duration, Figure 5.5D. Time variation of particle translocations has been seen before in experiments in which particles passed through the pore via an externally applied pressure difference. It is known that if a pore is cylindrical in shape, the velocity profile will have the characteristic Poisseuille character, thus the fluid and particle velocity will depend on the position with respect to the pore axis. If different particles took different trajectories when passing through the pore, the observed translocation time would feature large dispersion. This suggests that the reason for the variation of the time duration seen in our experiments might reflect different trajectories that particles can take in our rough pores. To explore this idea further, more experiments were done with pores of different roughness and aspect ratios.

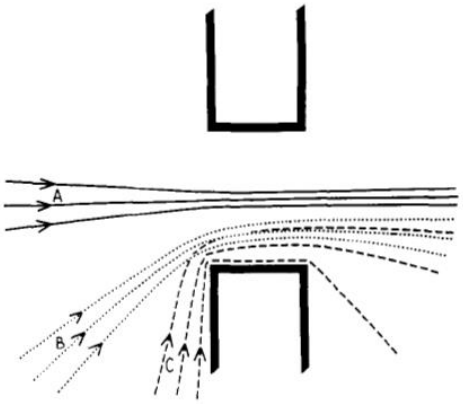

Figure 5.6: Visual respresentation of possible particle trajectories through a pore for a particle that has a 0 degree angle of approach (A), 45 degree angle of approach (B), and and 85 degree angle of approach [57].

The first set of pores that were analyzed had a range of aspect ratios from 2 to 11. This was to determine if increasing the number of possible trajectories for translocation could be one of the reasons for the increase in variation in event time duration. We expected that shorter pores would offer more trajectories for particles because passage through the pore in this case is also affected by the direction from which the particle approaches the pore, Figure 5.6. Histograms were used to compare the weighted average variance in translocation time for different experimental conditions and pores, Figure 5.7. The three shorter pores (pores 1-3) with aspect ratios of 3 or less showed higher dispersion times compared to previous particle experiments [54]. This phenomenon was particularly pronounced for particles that passed through in the direction of electroosmosis. Comparing experiments performed on short and long pores (pores 4,5) confirms that the lower aspect ratio increases translocation time variability, as the long pores had dispersion of less than 20%. The fact that aspect ratio plays a role in the dispersion of translocation times indicates that multiple particle trajectories increase the variability of translocation time.

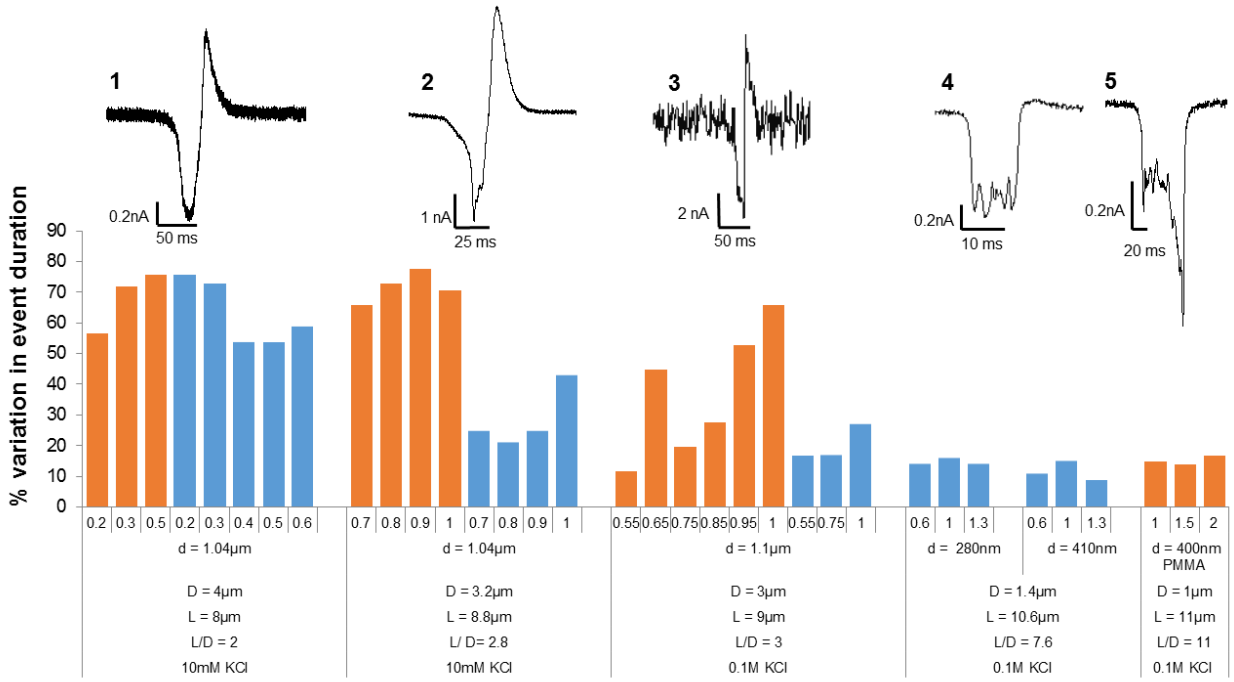

Figure 5.7: Histograms of percentage change in variance in event durations for 5 pores. The x-axis is the applied voltage in volts. The pores with the larger opening diameter (D) are shorter in length (L) as the material is etched away proportional to the pore diameter. The particle diameter is given by d. Blue and orange bars represent electrophoretic and electroosmotic transport of particles, respectively. The insets are example resistive pulse events for each pore. In order to find the percentage variability the square root of the variance was divided by the average. Both values were found with histograms. Pores 1,2,4, and 5 were measured on the Axopatch 200B. Pore 3 was measured with the custom built amplifier [39].

The next step was to determine whether the roughness of the pores plays a significant role in the dispersion of the translocation times, Figure 5.8. Roughness in the PET pores is understood as an axially varying diameter. All PET pores exhibit a certain level of variation, however some pores were especially rough as seen by large amplitudes of current changes within a resistive pulse, e.g. pore 6 in Figure 5.8; as expected, variability of translocation time through these pores was higher than through smoother pores. The second set of 6 pores shown in Figure 5.7, confirms the conclusions drawn from the pores shown in Figure 5.6, namely that pores with a lower aspect ratio also cause larger variation in the passage times.

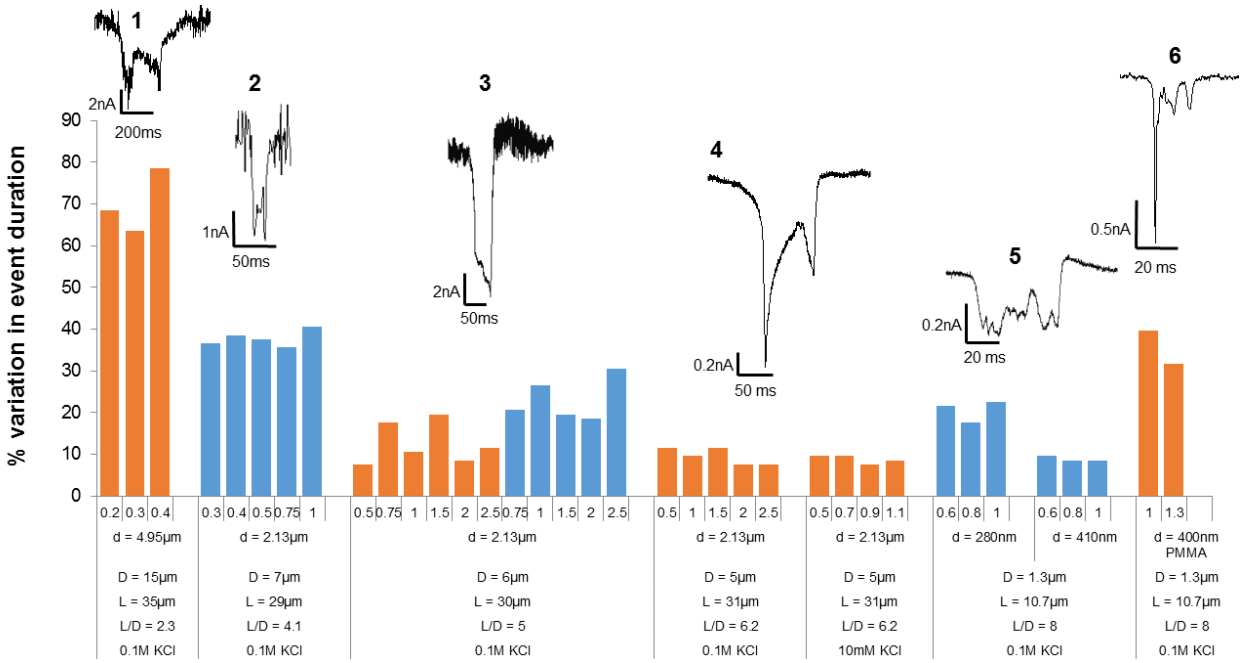

Figure 5.8: Dispersion of particle translocation times in six pores with variying opening diameter (D), length (L), and topography. On the x axis the applied voltage is in volts. Particle diameter is given by d. Blue and orange bars represent electrophoresis and electroomosis transport, respectively. The custom built amplifier was used to record data for pores 1-4 in 0.1 M KCl. The Axopatch 200B was used to record data for pore 4 in 10 mM KCl and all data for pores 5 and 6 [39].

To investigate why roughness played a role in the modulating the translocation times, the velocity profiles of electroosmosis in rough pores were modeled. Electroosmotic flow in a smooth cylindrical channel has a plug-like velocity profile, but that is not the case when roughness is added to the channel. Since the continuity equation must be fulfilled the fluid velocity in the narrow regions of the pore must be higher than in the wider regions. A consequence of this is the wider regions pull fluid from the narrow regions creating a local pressure difference. Inhomogeneous pressure drops and location dependent velocities profiles have been predicted and studied previously using smooth cylindrical pores with inhomogeneous zeta potentials [58]. In order to visualize the flow, a florescent dye was used. It was observed that the changing zeta potentials did indeed change the observed velocity profile so that no Poisseuille flow was observed. For our system the velocity profiles in a rough pore were modeled by numerically solving the coupled PNP

and NS equations for two types of pores. In one longer pore that had a length of 4.2 μm, the diameter of the narrow regions is 350 nm and the cavity has a diameter ranging from 450 to 750 nm. The shorter pore, which was 900 nm long, had a narrow region with a diameter of 350 nm and a cavity with diameter 550 nm. The surface charge of the pores was -0.5 e/nm^2 and the bulk electrolyte was 10 mM KCl for both cases.

Modeling performed for the long pore indicates the velocity field in the narrow regions is fairly flat with a local minima at the pore axis and maximums near the pore walls, Figure 5.9. This flow has been observed before in cylindrical pores with inhomogeneous zeta potential [58]. The wider region had a more complex velocity profile, where the maximum was at the pore axis and the local minimum was near the pore walls. For larger undulations this phenomenon was more pronounced. When the undulation is 750 nm in diameter, a = 200 nm, the liquid is almost stalled 100 nm from the pore walls. The middle region of the cavity is similar to the narrow regions. These velocity profiles suggest that the fluid next to the wall is unable to follow sharp corners. This modeling further confirmed the presence of local pressure gradients and that for larger undulations the pressure has a higher magnitude, Figure 5.9.

The modeling for the shorter pore with an aspect ratio of 3 had higher velocity magnitudes than the longer pore, Figure 5.10. This is due to the higher electric field produced with the same applied voltage. The narrow region is similar to the long pore, with the maxima near the pore walls and a local minima in the center of the pore. The velocity in the cavity has a local maxima in the center and two local maxima near the pore walls. However due to the undulation being comparable to the length of the segment the velocity profile does not flatten in the wide region. This modeling suggests that roughness does indeed play a significant role in modulating the translocation times

of particles. Increasing roughness makes the velocity profile more complex, thus depending on the trajectory the particle takes through the pore, it will translocate with different local velocities.

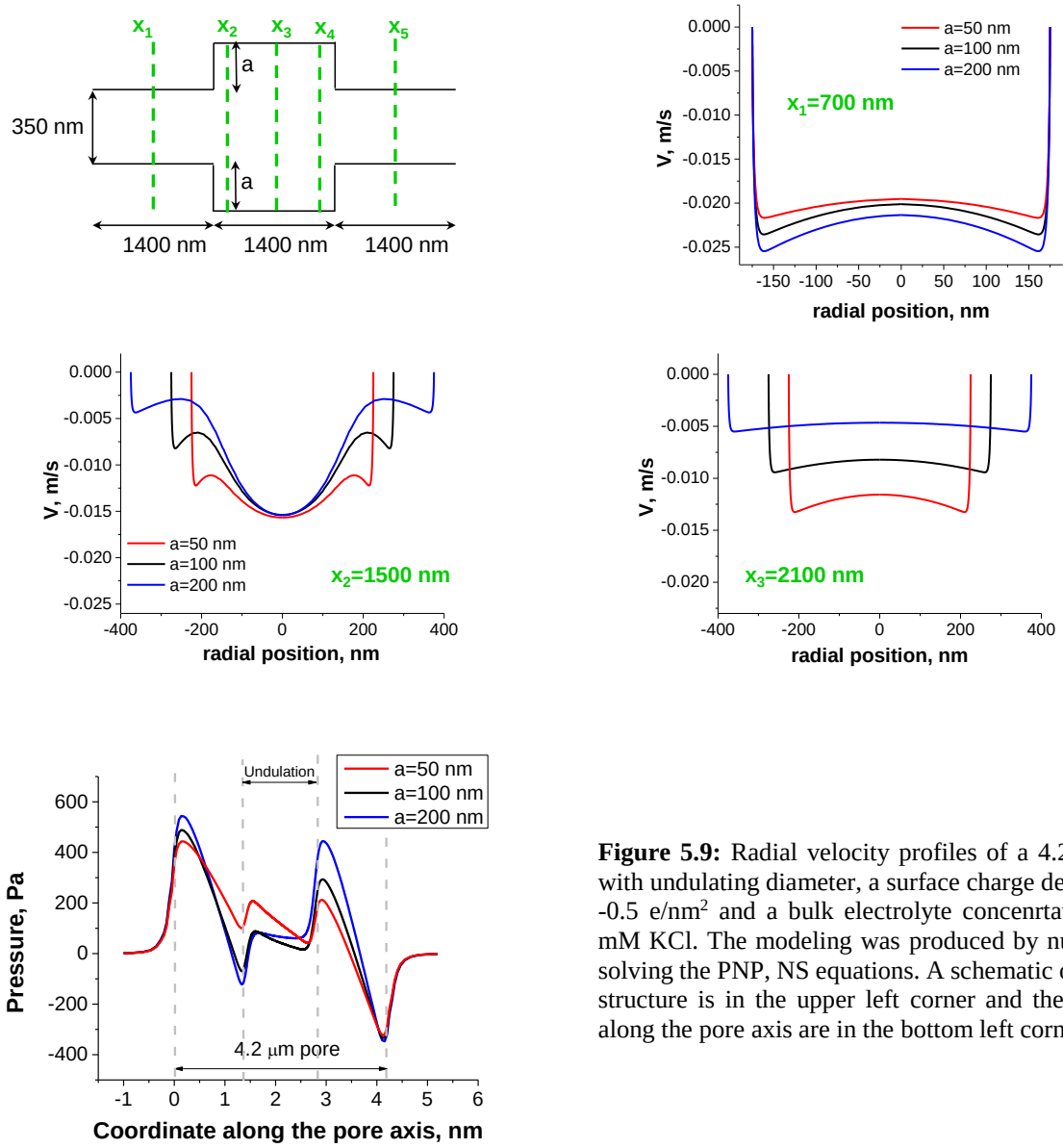

Figure 5.9: Radial velocity profiles of a 4.2 μm pore with undulating diameter, a surface charge density of -0.5 e/nm^2 and a bulk electrolyte concenrtation of 10 mM KCl. The modeling was produced by numerically solving the PNP, NS equations. A schematic of the pore structure is in the upper left corner and the pressures along the pore axis are in the bottom left corner. [39]

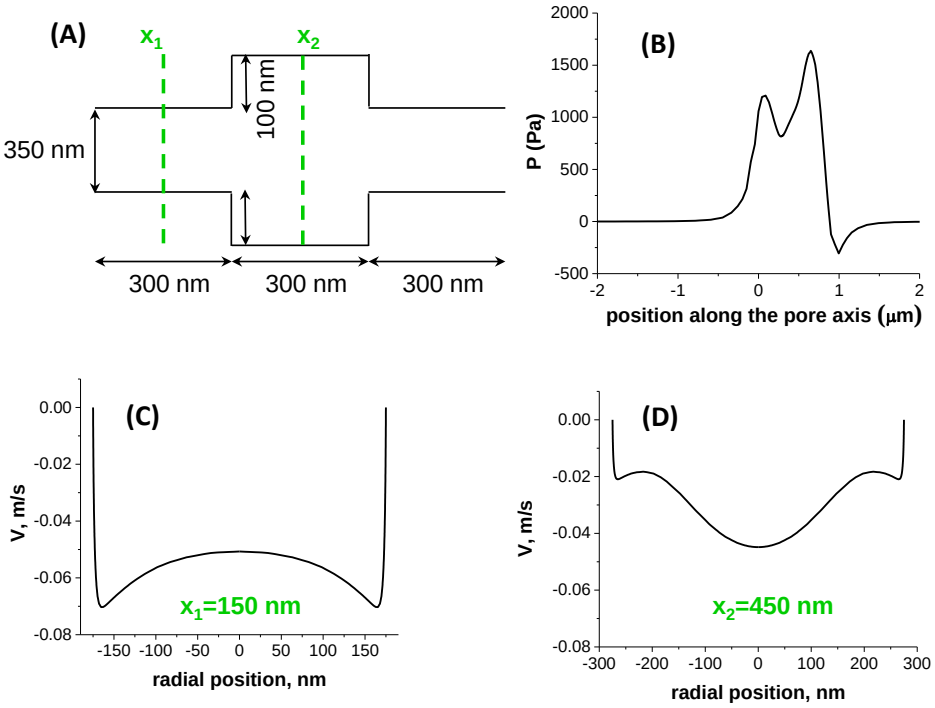

Figure 5.10: (A) Schematic of the short 900 nm pore **(B)** Pressure profile along the axis of the pore **(C)** Velocity profile along the narrow region **(D)** Velocity profile along the wide region [39].

The pressure gradients induced by the complex velocity profiles in the pore offer a possibility for non-contact deformation of soft particles. Experiments done by Pevarnik et al with negatively charged hydrogel particle experiments in similar PET pores to examine if this deformation was possible [59]. Hydrogels are spherical particles made from crosslinking monomers and are filled with ionic solution, KCl in this case. Hydrogels are of interest as they can collapse to a much smaller diameter than their original sizes, making them potentially useful as a drug delivery device. Hard spherical particles were first passed through the pore in order to determine the topography of the pore. The resistive pulse seen in Figure 5.11, consisted of two larger current decreases at both pore entrances and a shallower current decrease in the middle, indicating presence of a cavity. The hydrogel translocations produced pulses of a similar structure except there was an increase in current at the beginning of the event that traced the pore topography,

i.e. two narrow entrances and the cavity. This increase was followed by a blockage of the current. Presence of a hydrogel in the pore causes a current increase not decrease, because the hydrogel is filled with ionic solution; thus a hydrogel brings more ions into the pore than the number of ions it displaces. The current decrease at the end of the translocation was interpreted as hydrogel in its collapsed and dehydrated form. The hydrogel collapse was observed due to the pressure differences the particle is subjected to while translocating, Figure 5.9.

Since it was possible to deform the submicron hydrogels without physically touching them, it could also be possible to deform microscopic objects such as biological cells. This would be particularly interesting as physical abnormalities in cells are often indicative of diseases. The specific focus will be to determine if a system of rough pores is capable of detecting the squishiness/mechanical properties of individual circulating tumor cells (CTCs). As the ability to detect and separate CTCs without labeling would be very advantageous over existing characterization techniques.

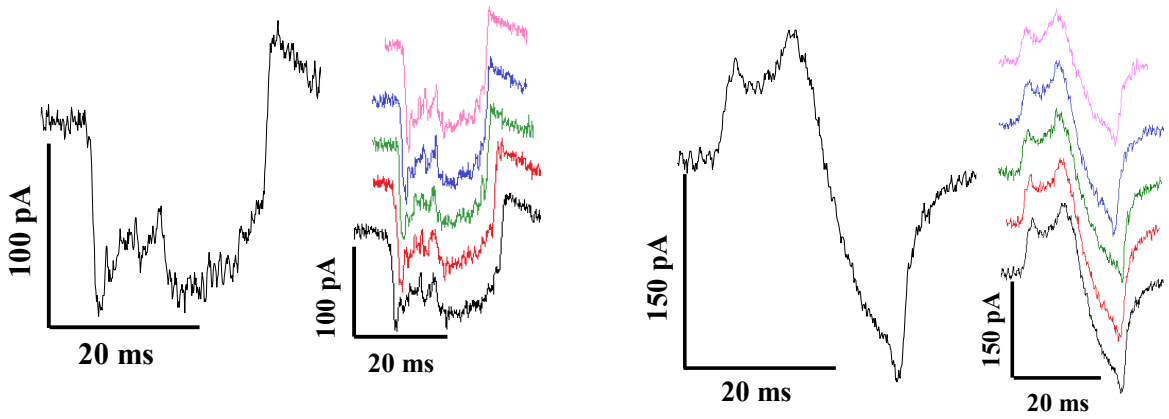

Figure 5.11: Hard sphere translocation of a 220 nm sphere through a 540 nm pore, where pore topography has two constrictions with a cavity in the middle, left side. 300 nm hydrogel translocation through the same pore, where topography is seen in the increase in current and there is pore blockage after the hydrogel deforms, right side [59].

Mouse J774A.1 macrophage cells from reticulum cell sarcoma were the first type of cells we detected and analyzed with single rough pores. A mixture of J774A.1 mouse cells and 5 μm

particles at concentrations of 10^4/mL and 10^8/mL, respectively, in PBS were placed on one side of the 15 µm pore with the working electrode. The cells and particles passed through the pore by electroosmosis. It is important to note that the concentrations of particles used for this set of experiments is just an order of magnitude below the concentration of red blood cells in whole blood. The cells were easily distinguishable from the particles as they are much larger than the particles, Figure 5.12. Passage of the particles again traced the topography of the pore indicating there was a constriction at the entrance and exit, with a cavity in the middle. It also indicted that the constrictions were of similar size, as the peaks in the particle events were close in size as well. A closer look at the mouse translocations indicated that the two peaks were not the same size. This suggests that the mouse cells were undergoing deformation as they passed through the pore. As these results with the mouse cells were quite promising, we wanted to try human cells next with longer pores.

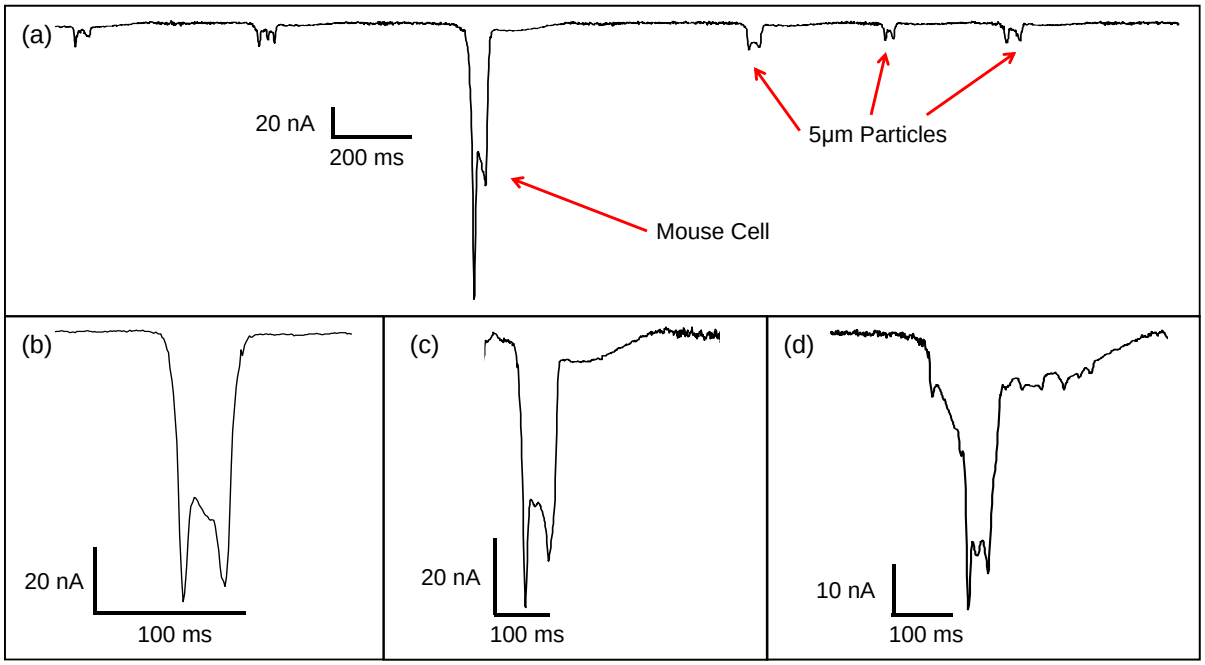

Figure 5.12: Top panel is examples of particle translocations with a single mouse cell translocation. The bottom panels are examples of other mouse cell translocations. The bottom right mouse cell translocation is a mouse cell event with particle translocations superimposed on top of it [39].

5.2.2 MCF-7 Cell Experiments

The first human cells that tested were breast cancer cells, specifically MCF-7. A set of experiments with four independently prepared pores was performed. Two PET pores with average diameters of 20 and 25 µm and lengths of 30 and 25 µm, respectively, and two polycarbonate (PC) pores with average diameters of 25 and 20 µm and lengths of 75 and 80 µm were used in the experiments. The cells were detected from a suspension containing ~10^6 cells/mL and prepared in an HBSS buffer with 0.1% pluronic. Pluronic is used to prevent the cells from sticking to each other or to surfaces thus it played a role of a surfactant. The same pores were used to detect polystyrene particles 10 µm in diameter present at a concentration of ~ 10^8 per mL with 0.1% Tween 80. In this thesis we will show data collected with the 25 µm diameter PC pore. Passage of the particles allowed us to trace the pore 3D topography and revealed that this PC pore had a similar geometry to the one used for the detection of mouse cells, namely it contained two constrictions of roughly the same diameter and a cavity in the middle, Figure 5.13A. The particle events were also used to calculate the diameter of the undulations and it was determined that the constrictions had a diameter of 21 µm and the cavity had a diameter of 23 µm. A 2D visual representation of the pore topography is shown in Figure 5.13B.

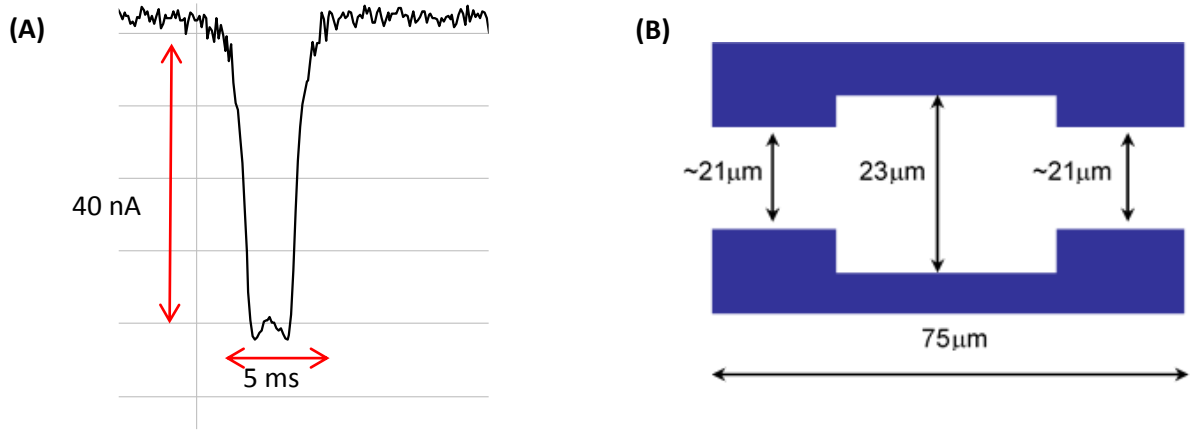

Figure 5.13: A) Current pulse of a 10 µm particle through the 25 µm pore. **B)** Schematic of the topography of the 25 µm PC pore based on particle events.

Once the geometry of the pore was known the cells were translocated electroosmotically through the pore and their individual current pulses were recorded. The individual current pulses for the cells do not have the same peak heights like the particle events do. This indicates that the cells represent a heterogeneous population while the particles are homogeneous. Figure 5.14 contains three examples of cell translocations, where each represents cells of different sizes as evidenced by the differences in initial peak heights. After the cells were translocated through the pore they were removed from the conductivity cell with a sterile pipette and plated. The cell growth was observed for 9 days. The experiments provided evidence the detected cells remained viable after translocation through the pore, Figure 5.14.

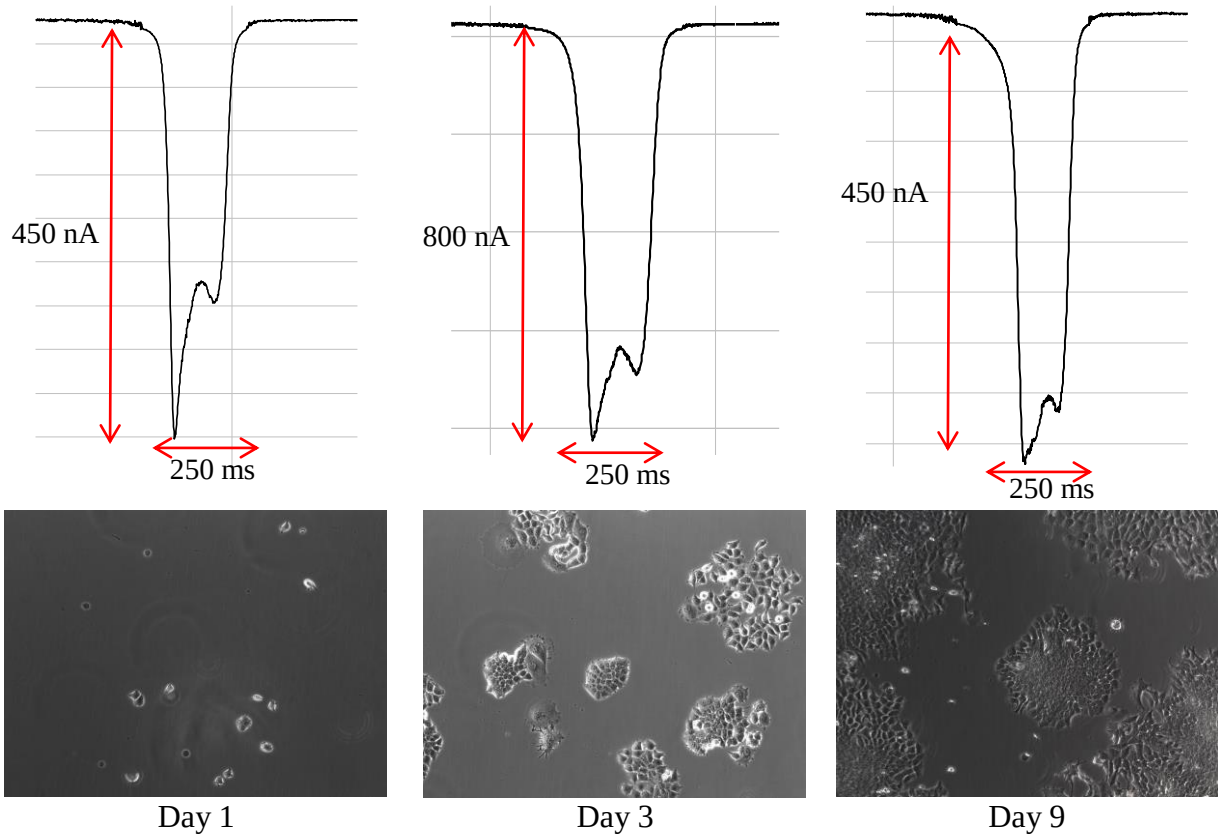

Figure 5.14: Top: Examples of three different MCF-7 cell translocations. **Bottom:** MCF-7 cells were plated after being translocated through the 25 µm PC pore. Images were taken with an inverted Olympus IX70 microscope using the SPOT Idea 3.0 camera and Spot acquisition software (Spot Imagining Solutions) on the day the cells were plated (Day 1) and then again on Day 3 and Day 9. Cell growth is seen in both Day 3 and Day 9 images.

Passage of ~200 cells was observed and analyzed using a custom Matlab program. The pulses created by the cells and local ion current changes were used to determine if the cells changed their size while translocating. The difference in size between the first peak and the second peak were examined. However there was no correlation, so the next step was to look at the difference in size between the first peak and the cavity. Here there was indication of size change, red bars in the histrogram in Figure 5.15. There is a wide variation in size change for the cells. This is expected as the population of MCF-7 cells are heterogeneous. For comparison fixed MCF-7 cells were also translocated through the pore. Fixed cell are dead cells that were incubated with 4% paraformaldehyde for 30 minutes to keep them from degrading. The fixed cells are expected to be more rigid than the live MCF-7 cells. While there is overlap of the fixed cells and the live cells in the histogram, the fixed cells tend to squish to a much smaller extent. This indicates that the fixed cells are less deformable than the live MCF-7 cells. These are very promising results, but a larger difference in the deformation of fixed cells and viable cells would allow for better detection. It is possible that this can be achieved by using a pore with a larger undulation, thus applying more pressure. Future experiments will explore this idea.

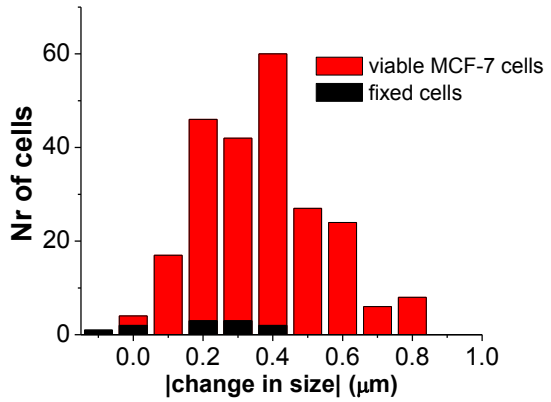

Figure 5.15: Histrogram of the change of cell diameter from peak one to the cavity. Red bars represented the live cells and black bars represented the fixed cells.

Chapter 6
Conclusions

In this thesis I have discussed the fabrication of polymer pores, ion transport through the pores, hydrophobic gating, and particle and cell translocations. Polymer pores were irradiated with a single swift heavy, creating a damage track in the foil. The damage track was then etched to create either a conical or a cylindrical nanopore by controlling the bulk and track etch rates. The processes of etching polyethylene terephthalate (PET) or polycarbonate (PC) creates negatively charged carboxyl groups on the pore walls, which increase the salt concentration inside the pore to above bulk. The increase of salt concentration in the pores leads to higher currents and in conical nanopores rectification of the ion current. Ion current behaviors in polymer pores can be controlled electrostatically or with hydrophobic interactions. It was also shown that smooth micropores created a plug-like electroosmotic flow.

The first experiments discussed were hydrophobic gating with single conical nanopores. Conical nanopores created in PET were modified with C3, C6, and C10 alkyl chains to study the effect of chain length on hydrophobic gating. Planar PET surfaces were also modified in the same manner as the nanopores and contact angle measurements were performed. While the unmodified PET surface had a low contact angle, the modified surfaces all had similar contact angles. Naopores modified with the shorter alkyl chains exhibited only modest gating in 10 mM KCl, and were open for all other KCl concentrations. However, nanopores modified with the longest of the three alkyl chains, C10, were mostly closed in 10 mM KCl and gated in 100 mM and 1 M KCl. These pores also were able to repeatable gate, a behavior nanopores modified with C3 and C6 did not exhibit. It was also shown that the gating behavior was not only voltage dependent, but KCl concentration dependent as well. The salt concentration dependence was described by the outward stress on the meniscus which originated from the Maxwell and osmotic stress components. It was also shown that those stresses lead to electrocapillarity and modulation of the shape of the liquid vapor interface. Furthermore gating only occurred in nanopores that were partially modified, as previous experiments with partially modified pores never opened.

Experiments were also done with PC and PET micropores in attempts to extend the resistive pulse technique beyond sizing meso and micro sized objects. Polystyrene spheres were translocated through micropores by both electroosmosis and electrophoresis. It was found that the undulating diameter of the micropore produces electroosmotic velocities that were both radially and axially dependent. Thus pores with surface charge and axially varying diameters produce a wide distribution of particle translocation times. This effect is especially pronounced in pores with a low aspect ratio or pores that are very rough. Modeling of rough pores indicated a dependence on the length of the undulations and the stability of the velocity profile. The velocity profile of

short undulations had a radially dependent velocity throughout the whole undulation. However with the long undulation the velocity profile eventually stabilizes exhibiting little radial variability. This produces a powerful analytical tool as the complex velocity fields produce pressure gradients inside the pore. Experiments with biological cells and hydrogels suggest the pressure gradients produced are large enough to cause deformation of translocated objects. Information gleamed from the deformation of an object can provide insight into its mechanical properties. Thus pores with an undulating diameter offer a possibility to extend the resistive pulse technique beyond sizing to provide a high-throughput method for probing the mechanical properties of meso to micro sized objects.

References

[1] Z. Siwy, P. Apel, D. Baur, D. D. Dobrev, Y. E. Korchev, R. Neumann, R. Spohr, C. Trautmann, and K.-O. Voss, "Preparation of synthetic nanopores with transport properties analogous to biological channels," *Surf. Sci.*, vol. 532–535, pp. 1061–1066, Jun. 2003.

[2] L. Innes, M. R. Powell, I. Vlassiouk, C. Martens, and Z. S. Siwy, "Precipitation-Induced Voltage-Dependent Ion Current Fluctuations in Conical Nanopores," *J. Phys. Chem. C*, vol. 114, no. 18, pp. 8126–8134, May 2010.

[3] O. Beckstein and M. S. P. Sansom, "A hydrophobic gate in an ion channel: the closed state of the nicotinic acetylcholine receptor.," *Phys. Biol.*, vol. 3, no. 2, pp. 147–59, Jun. 2006.

[4] M. Ø. Jensen, D. W. Borhani, K. Lindorff-Larsen, P. Maragakis, V. Jogini, M. P. Eastwood, R. O. Dror, and D. E. Shaw, "Principles of conduction and hydrophobic gating in K+ channels.," *Proc. Natl. Acad. Sci. U. S. A.*, vol. 107, no. 13, pp. 5833–8, Mar. 2010.

[5] I. Vlassiouk and Z. S. Siwy, "Nanofluidic diode.," *Nano Lett.*, vol. 7, no. 3, pp. 552–6, Mar. 2007.

[6] S. Mitragotri and J. Lahann, "Physical approaches to biomaterial design.," *Nat. Mater.*, vol. 8, no. 1, pp. 15–23, 2009.

[7] M. D. Graham, "The Coulter Principle: Foundation of an industry," *JALA - J. Assoc. Lab. Autom.*, vol. 8, no. 6, pp. 72–81, 2003.

[8] T. M. Squires and S. R. Quake, “Microfluidics: Fluid physics at the nanoliter scale,” *Rev. Mod. Phys.*, vol. 77, no. July, 2005.

[9] S. Huang, H. Bow, M. Diez-silva, and J. Han, “Applying A Microfluidic ‘Deformability Cytometry’ To Measure Stiffness of Malaria Infected Red Blood Cells at Body and Febrile Temperatures,” *14th Int. Conf. Miniaturized Syst. Chem. Life Sci.*, no. October, pp. 259–261, 2010.

[10] T. Asakura, J. a Mattiello, K. Obata, K. Asakura, M. P. Reilly, N. Tomassini, E. Schwartz, and K. Ohene-Frempong, “Partially oxygenated sickled cells: sickle-shaped red cells found in circulating blood of patients with sickle cell disease.,” *Proc. Natl. Acad. Sci. U. S. A.*, vol. 91, no. 26, pp. 12589–12593, 1994.

[11] G. Vona, a Sabile, M. Louha, V. Sitruk, S. Romana, K. Schütze, F. Capron, D. Franco, M. Pazzagli, M. Vekemans, B. Lacour, C. Bréchot, and P. Paterlini-Bréchot, “Isolation by size of epithelial tumor cells : a new method for the immunomorphological and molecular characterization of circulatingtumor cells.,” *Am. J. Pathol.*, vol. 156, no. 1, pp. 57–63, 2000.

[12] W. Xu, R. Mezencev, B. Kim, L. Wang, J. McDonald, and T. Sulchek, “Cell Stiffness Is a Biomarker of the Metastatic Potential of Ovarian Cancer Cells,” *PLoS One*, vol. 7, no. 10, 2012.

[13] Z. Siwy, M. E. Mycielska, and M. B. a Djamgoz, “Statistical and fractal analyses of rat prostate cancer cell motility in a direct current electric field: comparison of strongly and weakly metastatic cells.,” *Eur. Biophys. J.*, vol. 32, no. 1, pp. 12–21, 2003.

[14] S. Park, R. R. Ang, S. P. Duffy, J. Bazov, K. N. Chi, P. C. Black, and H. Ma, “Morphological differences between circulating tumor cells from prostate cancer patients and cultured prostate cancer cells,” *PLoS One*, vol. 9, no. 1, 2014.

[15] S. Applications, *Handbook of Single-Molecule Biophysics*. New York, NY: Springer US, 2009.

[16] M. Ø. Jensen, V. Jogini, D. W. Borhani, A. E. Leffler, R. O. Dror, and D. E. Shaw, “Mechanism of voltage gating in potassium channels.,” *Science*, vol. 336, no. 6078, pp. 229–33, Apr. 2012.

[17] S. Sukharev and A. Anishkin, “Mechanosensitive channels: what can we learn from ‘simple’ model systems?,” *Trends Neurosci.*, vol. 27, no. 6, pp. 345–51, Jun. 2004.

[18] D. a Doshi, E. B. Watkins, J. N. Israelachvili, and J. Majewski, “Reduced water density at hydrophobic surfaces: effect of dissolved gases.,” *Proc. Natl. Acad. Sci. U. S. A.*, vol. 102, no. 27, pp. 9458–62, Jul. 2005.

[19] A. Luzar, “Activation Barrier Scaling for the Spontaneous Evaporation of Confined Water †,” pp. 19859–19866, 2004.

[20] B. Lefevre, a Saugey, J. L. Barrat, L. Bocquet, E. Charlaix, P. F. Gobin, and G. Vigier, “Intrusion and extrusion of water in hydrophobic mesopores.,” *J. Chem. Phys.*, vol. 120, no. 10, pp. 4927–38, Mar. 2004.

[21] L. Guillemot, T. Biben, A. Galarneau, G. Vigier, and É. Charlaix, “Activated drying in hydrophobic nanopores and the line tension of water.,” *Proc. Natl. Acad. Sci. U. S. A.*, vol. 109, no. 48, pp. 19557–62, 2012.

[22] M. R. Powell, L. Cleary, M. Davenport, K. J. Shea, and Z. S. Siwy, “Electric-field-induced wetting and dewetting in single hydrophobic nanopores.,” *Nat. Nanotechnol.*, vol. 6, no. 12, pp. 798–802, Dec. 2011.

[23] S. N. Smirnov, I. V Vlassiouk, and N. V Lavrik, “Voltage-Gated Hydrophobic Nanopores,” no. 9, pp. 7453–7461, 2011.

[24] D. Wirtz, K. Konstantopoulos, and P. C. Searson, “The physics of cancer: the role of physical interactions and mechanical forces in metastasis.,” *Nat. Rev. Cancer*, vol. 11, no. 7, pp. 512–522, 2011.

[25] M. C. Miller, G. V Doyle, and L. W. M. M. Terstappen, “Significance of Circulating Tumor Cells Detected by the CellSearch System in Patients with Metastatic Breast Colorectal and Prostate Cancer.,” *J. Oncol.*, vol. 2010, p. 617421, 2010.

[26] H. K. Lin, S. Zheng, A. J. Williams, M. Balic, S. Groshen, H. I. Scher, M. Fleisher, W. Stadler, R. H. Datar, Y. C. Tai, and R. J. Cote, “Portable filter-based microdevice for detection and characterization of circulating tumor cells,” *Clin. Cancer Res.*, vol. 16, no. 20, pp. 5011–5018, 2010.

[27] D. L. Adams, S. S. Martin, R. K. Alpaugh, M. Charpentier, S. Tsai, R. C. Bergan, I. M. Ogden, W. Catalona, S. Chumsri, C.-M. Tang, and M. Cristofanilli, “Circulating giant macrophages as a potential biomarker of solid tumors.,” *Proc. Natl. Acad. Sci. U. S. A.*, vol. 111, no. 9, pp. 3514–9, 2014.

[28] J. Guck, S. Schinkinger, B. Lincoln, F. Wottawah, S. Ebert, M. Romeyke, D. Lenz, H. M. Erickson, R. Ananthakrishnan, D. Mitchell, J. Käs, S. Ulvick, and C. Bilby, “Optical deformability as an inherent cell marker for testing malignant transformation and metastatic competence.,” *Biophys. J.*, vol. 88, no. 5, pp. 3689–3698, 2005.

[29] Q. S. Li, G. Y. H. Lee, C. N. Ong, and C. T. Lim, “AFM indentation study of breast cancer cells.,” *Biochem. Biophys. Res. Commun.*, vol. 374, no. 4, pp. 609–13, Oct. 2008.

[30] S. Byun, S. Son, D. Amodei, N. Cermak, J. Shaw, J. H. Kang, V. C. Hecht, M. M. Winslow, T. Jacks, P. Mallick, and S. R. Manalis, “Characterizing deformability and

surface friction of cancer cells.," *Proc. Natl. Acad. Sci. U. S. A.*, vol. 110, no. 19, pp. 7580–5, 2013.

[31] R. Spohr, *Ion Tracks and Microtechnology Principles and Applications*. Braunschweig: Vieweg & Sohn Verlagsgesellschaft, 1990.

[32] R. Spohr, "United States Patent [19]," 1983.

[33] W. Desorbo, "Ultraviolet Effects and Aging Effects on Etching Characteristics of Fission Tracks in Polycarbonate Film," *Nucl. Tracks*, vol. 3, pp. 13–32, 1979.

[34] V. Chavan, C. Agarwal, A. K. Pandey, J. P. Nair, P. Surendran, P. C. Kalsi, and a. Goswami, "Controlled development of pores in polyethylene terepthalate sheet by room temperature chemical etching method," *J. Memb. Sci.*, vol. 471, pp. 185–191, 2014.

[35] P. Y. Apel, Y. . Korchev, Z. Siwy, R. Spohr, and M. Yoshida, "Diode-like single-ion track membrane prepared by electro-stopping," *Nucl. Instruments Methods Phys. Res. Sect. B Beam Interact. with Mater. Atoms*, vol. 184, no. 3, pp. 337–346, Nov. 2001.

[36] C. C. Harrell, Z. S. Siwy, and C. R. Martin, "Conical nanopore membranes: controlling the nanopore shape.," *Small*, vol. 2, no. 2, pp. 194–8, Feb. 2006.

[37] P. Scopece, L. a Baker, P. Ugo, and C. R. Martin, "Conical nanopore membranes: solvent shaping of nanopores," *Nanotechnology*, vol. 17, no. 15, pp. 3951–3956, Aug. 2006.

[38] M. R. Powell, C. Martens, and Z. S. Siwy, "Asymmetric properties of ion current 1/f noise in conically shaped nanopores," *Chem. Phys.*, vol. 375, no. 2–3, pp. 529–535, 2010.

[39] L. M. Innes, C. Chen, M. Schiel, M. Pevarnik, F. Haurais, M. E. Toimil-molares, I. Vlassiouk, L. Theogarajan, and Z. S. Siwy, "Velocity Pro fi les in Pores with Undulating Opening Diameter and Their Importance for Resistive-Pulse Experiments," *Anal. Chem.*, vol. 85, pp. 10445–10453, 2014.

[40] E. Kalman, "Control of Ion Current Rectification in Asymmetric Nanopores by Signal Mixing by," 2009.

[41] I. Vlassiouk, S. Smirnov, and Z. Siwy, "Ionic selectivity of single nanochannels.," *Nano Lett.*, vol. 8, no. 7, pp. 1978–85, Jul. 2008.

[42] M. R. Powell, I. Vlassiouk, C. Martens, and Z. S. Siwy, "Nonequilibrium 1/f Noise in Rectifying Nanopores," *Phys. Rev. Lett.*, vol. 103, no. 24, p. 248104, Dec. 2009.

[43] S. Smirnov, I. Vlassiouk, P. Takmakov, and F. Rios, "Water Confinement in Hydrophobic Nanopores. Pressure-Induced Wetting and Drying," *ACS Nano*, vol. 4, no. 9, pp. 5069–5075, 2010.

[44] M. a Pevarnik, “Transport of Ions and Particles Through Single Pores of Controlled Geometry and Surface Chemistry,” 2012.

[45] I. Vlassiouk, T. R. Kozel, and Z. S. Siwy, “Biosensing with nanofluidic diodes,” *J. Am. Chem. Soc.*, vol. 131, no. 23, pp. 8211–8220, 2009.

[46] L. Innes, D. Gutierrez, W. Mann, S. F. Buchsbaum, and Z. S. Siwy, “Presence of electrolyte promotes wetting and hydrophobic gating in nanopores with residual surface charges,” *Analyst*, 2015.

[47] L. Innes, “Hydrophobic Gating in Single and Multiple Nanopores,” 2014.

[48] L. Liu, X. Chen, W. Lu, A. Han, and Y. Qiao, “Infiltration of electrolytes in molecular-sized nanopores,” *Phys. Rev. Lett.*, vol. 102, no. 18, pp. 1–4, 2009.

[49] J. Dzubiella and J.-P. Hansen, “Electric-field-controlled water and ion permeation of a hydrophobic nanopore.,” *J. Chem. Phys.*, vol. 122, no. 23, p. 234706, Jul. 2005.

[50] R. Zangi, M. Hagen, and B. J. Berne, “Effect of ions on the hydrophobic interaction between two plates.,” *J. Am. Chem. Soc.*, vol. 129, no. 15, pp. 4678–86, Apr. 2007.

[51] J. a. Lee and I. S. Kang, “Electrocapillarity of an electrolyte solution in a nanoslit with overlapped electric double layer: Continuum approach,” *Phys. Rev. E*, vol. 90, no. 3, p. 032401, Sep. 2014.

[52] R. W. DeBlois and C. P. Bean, “Counting and sizing of submicron particles by the resistive pulse technique,” *Rev. Sci. Instrum.*, vol. 41, no. 7, pp. 909–916, 1970.

[53] Y. Qiu, P. Hinkle, C. Yang, H. E. Bakker, M. Schiel, H. Wang, D. Melnikov, M. Gracheva, M. E. Toimil-molares, A. Imhof, and Z. S. Siwy, “Pores with Longitudinal Irregularities Distinguish Objects by Shape,” *ACS Nano*, vol. 9, no. 4, pp. 4390–4397, 2015.

[54] M. Pevarnik, K. Healy, M. E. Toimil-Molares, A. Morrison, S. E. Létant, and Z. S. Siwy, “Polystyrene particles reveal pore substructure as they translocate.,” *ACS Nano*, vol. 6, no. 8, pp. 7295–302, Aug. 2012.

[55] C. Chen, S. Yemenicioglu, A. Uddin, E. Corgliano, and L. Theogarajan, “A CMOS enhanced solid-state nanopore based single molecule detection platform,” *Proc. Annu. Int. Conf. IEEE Eng. Med. Biol. Soc. EMBS*, pp. 164–167, 2013.

[56] J. Menestrina, C. Yang, M. Schiel, I. Vlassiouk, and Z. S. Siwy, “Charged particles modulate local ionic concentrations and cause formation of positive peaks in resistive-pulse-based detection,” *J. Phys. Chem. C*, vol. 118, no. 5, pp. 2391–2398, 2014.

[57] R. B. Adams and E. C. Gregg, “Pulse shapes from particles traversing Coulter orifice fields.,” *Phys. Med. Biol.*, vol. 17, no. 6, pp. 830–842, 1972.

[58] a. E. Herr, J. I. Molho, J. G. Santiago, M. G. Mungal, T. W. Kenny, and M. G. Garguilo, “Electroosmotic capillary flow with nonuniform zeta potential,” *Anal. Chem.*, vol. 72, no. 5, pp. 1053–1057, 2000.

[59] M. Pevarnik, M. Schiel, K. Yoshimatsu, I. V. Vlassiouk, J. S. Kwon, K. J. Shea, and Z. S. Siwy, “Particle deformation and concentration polarization in electroosmotic transport of hydrogels through pores,” *ACS Nano*, vol. 7, no. 4, pp. 3720–3728, 2013.